

¹ **Measurement of the Drell-Yan Absolute Cross-Section
in pp Collisions with a 120 GeV Proton Beam at
Fermilab**

⁴ Chatura Kuruppu¹, Stephen Pate-Morales¹

⁵ ¹New Mexico State University, Las Cruces, NM 88003, USA

⁶ October 2, 2025

⁷ **Abstract**

⁸ The proton-induced Drell-Yan process is a powerful experimental tool for probing the
⁹ antiquark distributions within nucleons. While existing data have extensively covered the
¹⁰ region of small parton momentum fraction (x), the SeaQuest experiment at Fermilab extends
¹¹ the kinematic reach to larger x values by utilizing a 120 GeV proton beam. In this work,
¹² we report the measurement of the double-differential Drell-Yan cross-sections, $d^2\sigma/dx_F dM$,
¹³ from collisions of protons with both liquid deuterium ($p+d$) and liquid hydrogen ($p+p$) tar-
¹⁴ getters. These measurements provide direct sensitivity to the $\bar{u}(x) + \bar{d}(x)$ and $\bar{u}(x)$ antiquark
¹⁵ distributions of the proton, respectively. The results are compared with theoretical predic-
¹⁶ tions from Quantum Chromodynamics (QCD) using several current parameterizations of
¹⁷ the proton's parton distribution functions. Additionally, these new data are compared with
¹⁸ previous measurements to examine the scaling behavior of the Drell-Yan cross-section across
¹⁹ a broad range of the kinematic variable $\sqrt{\tau}$.

²⁰ This work was supported in part by US DOE grant DE-FG02-94ER40847.

21 Contents

22	1	Introduction	5
23	2	Analysis Methodology	5
24	2.1	Data and Monte Carlo Samples	5
25	2.2	Event Selection	6
26	2.3	Cross-Section Formalism	6
27	3	Acceptance and Efficiency Corrections	7
28	3.1	Detector Acceptance Correction	7
29	3.2	Reconstruction Efficiency Correction	24
30	3.2.1	Uncertainty Propagation	24
31	3.2.2	Efficiency Results	24
32	4	Systematic Uncertainties	45
33	5	Results: Double-Differential Cross-Section	45
34	6	Discussion and Conclusion	63
35	A	Appendix: Event Selection Criteria	64
36	A.1	Positive Track Cuts (<code>chuckCutsPositive_2111v42</code>)	64
37	A.2	Negative Track Cuts (<code>chuckCutsNegative_2111v42</code>)	64
38	A.3	Dimuon Cuts (<code>chuckCutsDimuon_2111v42</code>)	64
39	A.4	Physics and Occupancy Cuts	64

40 List of Figures

41	1	Acceptance plots for $0.00 \leq x_F < 0.05$	8
42	2	Acceptance plots for $0.05 \leq x_F < 0.10$	9
43	3	Acceptance plots for $0.10 \leq x_F < 0.15$	10
44	4	Acceptance plots for $0.15 \leq x_F < 0.20$	11
45	5	Acceptance plots for $0.20 \leq x_F < 0.25$	12
46	6	Acceptance plots for $0.25 \leq x_F < 0.30$	13
47	7	Acceptance plots for $0.30 \leq x_F < 0.35$	14
48	8	Acceptance plots for $0.35 \leq x_F < 0.40$	15
49	9	Acceptance plots for $0.40 \leq x_F < 0.45$	16
50	10	Acceptance plots for $0.45 \leq x_F < 0.50$	17
51	11	Acceptance plots for $0.50 \leq x_F < 0.55$	18
52	12	Acceptance plots for $0.55 \leq x_F < 0.60$	19
53	13	Acceptance plots for $0.60 \leq x_F < 0.65$	20
54	14	Acceptance plots for $0.65 \leq x_F < 0.70$	21
55	15	Acceptance plots for $0.70 \leq x_F < 0.75$	22
56	16	Acceptance plots for $0.75 \leq x_F < 0.80$	23
57	17	Efficiency plots for the x_F bin $0.00 \leq x_F < 0.05$	25
58	18	Efficiency plots for the x_F bin $0.05 \leq x_F < 0.10$	26
59	19	Efficiency plots for the x_F bin $0.10 \leq x_F < 0.15$	27
60	20	Efficiency plots for the x_F bin $0.15 \leq x_F < 0.20$	28
61	21	Efficiency plots for the x_F bin $0.20 \leq x_F < 0.25$	29
62	22	Efficiency plots for the x_F bin $0.25 \leq x_F < 0.30$	30
63	23	Efficiency plots for the x_F bin $0.30 \leq x_F < 0.35$	31
64	24	Efficiency plots for the x_F bin $0.35 \leq x_F < 0.40$	32
65	25	Efficiency plots for the x_F bin $0.40 \leq x_F < 0.45$	33
66	26	Efficiency plots for the x_F bin $0.45 \leq x_F < 0.50$	34
67	27	Efficiency plots for the x_F bin $0.50 \leq x_F < 0.55$	35
68	28	Efficiency plots for the x_F bin $0.55 \leq x_F < 0.60$	36
69	29	Efficiency plots for the x_F bin $0.60 \leq x_F < 0.65$	37
70	30	Efficiency plots for the x_F bin $0.65 \leq x_F < 0.70$	38
71	31	Efficiency plots for the x_F bin $0.70 \leq x_F < 0.75$	39
72	32	Efficiency plots for the x_F bin $0.75 \leq x_F < 0.80$	40
73	33	Efficiency plots for the x_F bin $0.80 \leq x_F < 0.85$	41
74	34	Differential cross-section for x_F bin $0.00 \leq x_F < 0.05$	47
75	35	Differential cross-section for x_F bin $0.05 \leq x_F < 0.10$	48
76	36	Differential cross-section for x_F bin $0.10 \leq x_F < 0.15$	49
77	37	Differential cross-section for x_F bin $0.15 \leq x_F < 0.20$	50
78	38	Differential cross-section for x_F bin $0.20 \leq x_F < 0.25$	51
79	39	Differential cross-section for x_F bin $0.25 \leq x_F < 0.30$	52
80	40	Differential cross-section for x_F bin $0.30 \leq x_F < 0.35$	53
81	41	Differential cross-section for x_F bin $0.35 \leq x_F < 0.40$	54
82	42	Differential cross-section for x_F bin $0.40 \leq x_F < 0.45$	55
83	43	Differential cross-section for x_F bin $0.45 \leq x_F < 0.50$	56
84	44	Differential cross-section for x_F bin $0.50 \leq x_F < 0.55$	57
85	45	Differential cross-section for x_F bin $0.55 \leq x_F < 0.60$	58
86	46	Differential cross-section for x_F bin $0.60 \leq x_F < 0.65$	59
87	47	Differential cross-section for x_F bin $0.65 \leq x_F < 0.70$	60
88	48	Differential cross-section for x_F bin $0.70 \leq x_F < 0.75$	61
89	49	Differential cross-section for x_F bin $0.75 \leq x_F < 0.80$	62

90 List of Tables

91	1	Average Efficiency and Errors for Bins in x_F and Mass	42
----	---	--	----

92 1 Introduction

93 The Drell-Yan process, where a quark from one hadron annihilates with an antiquark from
94 another to produce a lepton-antilepton pair ($q\bar{q} \rightarrow \ell^+\ell^-$), provides a clean and direct probe
95 of the antiquark structure of nucleons. Over the past several decades, Drell-Yan experiments
96 have been instrumental in mapping the parton distribution functions (PDFs) of the proton and
97 other hadrons. However, most existing data are concentrated at small to moderate values of
98 the parton momentum fraction, $x < 0.3$. The region of large x ($x > 0.3$) remains relatively
99 unexplored, yet it is crucial for understanding phenomena such as the flavor asymmetry of the
100 proton's light antiquark sea ($\bar{d}(x)/\bar{u}(x)$) and the fundamental mechanisms of non-perturbative
101 QCD that govern hadron structure.

102 The SeaQuest experiment (E906) at Fermilab was designed specifically to explore this high- x
103 frontier. By impinging a high-intensity 120 GeV proton beam from the Main Injector onto various
104 fixed targets, including liquid hydrogen (LH_2) and liquid deuterium (LD_2), SeaQuest measures
105 dimuon production in a kinematic region sensitive to antiquarks carrying a large fraction of the
106 nucleon's momentum.

107 This analysis presents a measurement of the absolute double-differential Drell-Yan cross-
108 section, binned in the dimuon invariant mass (M) and Feynman- x (x_F), using data collected
109 with the LH_2 and LD_2 targets. The p+p collisions are primarily sensitive to the \bar{u} distribution
110 in the proton, while the p+d collisions provide information on the sum of \bar{u} and \bar{d} . These results
111 provide stringent new constraints on modern PDF parameterizations in the valence-dominated
112 region.

113 The cross-section is presented in its scaling form, which, in the leading-order Drell-Yan
114 model, is independent of the center-of-mass energy, \sqrt{s} :

$$115 M^3 \frac{d^2\sigma}{dMdx_F} = f(\tau) \quad (1)$$

116 where $\tau = M^2/s$. The experimental determination of this quantity requires a precise under-
117 standing of the integrated luminosity, detector acceptance, and reconstruction efficiencies, which
118 are detailed in the subsequent sections of this document.

118 2 Analysis Methodology

119 The extraction of the Drell-Yan cross-section from the raw data involves several distinct steps:
120 selecting candidate dimuon events, subtracting backgrounds, calculating the integrated luminos-
121 ity, and correcting for detector- and reconstruction-related inefficiencies.

122 2.1 Data and Monte Carlo Samples

123 This analysis utilizes the "Roadset 67" dataset collected by the SeaQuest experiment. The
124 primary data files for the liquid hydrogen (LH_2) target and the corresponding empty "flask"
125 target runs are:

- 126 • **Data (LH_2 Target):** `merged_RS67_3089LH2.root`
- 127 • **Background (Empty Flask):** `merged_RS67_3089Flask.root`

128 The empty flask data are crucial for subtracting contributions from beam interactions with the
129 target vessel walls and other upstream material.

130 To correct for detector acceptance and reconstruction efficiencies, extensive Monte Carlo
131 (MC) simulations were employed. The simulations model the Drell-Yan process and propagate
132 the resulting muons through a Geant4-based model of the SeaQuest spectrometer. The primary
133 MC files used are:

- 134 • **Acceptance Study:** Drell-Yan events were generated over a 4π solid angle ("thrown")
 135 and also processed through the full detector simulation and reconstruction chain ("ac-
 136 cepted"). This study uses the *_M027_S001_* series of files:

```
137   – mc_drellyan_LH2_M027_S001_4pi_pTxFweight_v2.root  

  138   – mc_drellyan_LH2_M027_S001_clean_occ_pTxFweight_v2.root  

  139   – mc_drellyan_LH2_M027_S001_messy_occ_pTxFweight_v2.root  

  140   – mc_drellyan_LD2_M027_S001_4pi_pTxFweight_v2.root  

  141   – mc_drellyan_LD2_M027_S001_clean_occ_pTxFweight_v2.root  

  142   – mc_drellyan_LD2_M027_S001_messy_occ_pTxFweight_v2.root
```

- 143 • **Efficiency Study:** To model the effect of high detector occupancy on track reconstruction,
 144 simulated events were processed with ("messy") and without ("clean") the overlay of
 145 random background hits from experimental data. This study uses the *_M027_S002_*
 146 series of files:

```
147   – mc_drellyan_LH2_M027_S002_clean_occ_pTxFweight_v2.root  

  148   – mc_drellyan_LH2_M027_S002_messy_occ_pTxFweight_v2.root
```

149 All MC samples are weighted on an event-by-event basis to match the transverse momentum
 150 (p_T) distribution observed in the data.

151 2.2 Event Selection

152 A multi-tiered set of selection criteria is applied to isolate high-quality Drell-Yan dimuon events
 153 from the large background of other processes.

- 154 • **Data Quality:** Only data from "good spills," as identified by standard run quality moni-
 155 toring, are included in the analysis. A physics trigger condition (`MATRIX1 == 1`) is required,
 156 selecting events consistent with the passage of two muons through the spectrometer.
- 157 • **Track and Dimuon Quality:** A set of stringent cuts, developed by the collaboration and
 158 referred to as "Chuck cuts," are applied to ensure well-reconstructed positive and negative
 159 muon tracks that form a high-quality common vertex. These cuts impose requirements on
 160 track χ^2 , momentum, number of hits, and fiducial volume. The full details of these cuts
 161 are provided in Appendix A.
- 162 • **Kinematic Selection:** The analysis focuses on the high-mass continuum, away from the
 163 charmonium resonances ($J/\psi, \psi'$). A cut of $M_{\mu\mu} > 4.2$ GeV is applied. The analysis is
 164 restricted to the kinematic range $0 < x_F < 0.8$.

165 2.3 Cross-Section Formalism

166 The double-differential cross-section in a given kinematic bin ($\Delta M, \Delta x_F$) is calculated as:

$$\frac{d^2\sigma}{dMdx_F} = \frac{N_{DY}}{\Delta M \Delta x_F \cdot \mathcal{L} \cdot \epsilon_{\text{total}}} \quad (2)$$

167 where:

- N_{DY} is the number of Drell-Yan events in the bin after subtraction of the combinatoric
 and empty flask backgrounds (see [?] DocDB 11322).

$$N_{DY} = N_{\text{LH2}} - N_{\text{LH2, mixed}} - \frac{I_{\text{LH2}}}{I_{\text{flask}}} (N_{\text{flask}} - N_{\text{flask, mixed}})$$

- 168 • \mathcal{L} is the integrated luminosity for the dataset.
 169 • ϵ_{total} is the total correction factor, accounting for acceptance and inefficiencies.
- 170 The integrated luminosity, \mathcal{L} , is given by the product of the total number of protons incident
 171 on the target and the number of target nuclei per unit area:

$$\mathcal{L} = N_{\text{incident}} \cdot \frac{N_A \rho L}{A} \cdot f_{\text{atten}} \quad (3)$$

172 Here, N_{incident} is the number of protons on target, N_A is Avogadro's number, ρ is the target
 173 density, L is the target length, A is the molar mass, and f_{atten} is a correction factor for beam
 174 attenuation within the thick target. For the $L = 50.8$ cm long LH₂ target, with a density of
 175 $\rho_H = 0.0708$ g/cm³, the target thickness is 3.5966 g/cm² with a beam attenuation factor of
 176 0.966.

177 The total correction factor, ϵ_{total} , is the product of three terms determined from MC simu-
 178 lations:

$$\epsilon_{\text{total}} = \epsilon_{\text{acc}}(M, x_F) \cdot \epsilon_{\text{recon}}(M, x_F) \cdot \epsilon_{\text{trigger}} \quad (4)$$

179 where ϵ_{acc} is the geometric and kinematic acceptance of the spectrometer, ϵ_{recon} is the track
 180 reconstruction efficiency (often called "kTracker efficiency"), and $\epsilon_{\text{trigger}}$ is the trigger efficiency.
 181 The calculation of these three terms is detailed in the following sections.

182 3 Acceptance and Efficiency Corrections

183 3.1 Detector Acceptance Correction

184 The SeaQuest spectrometer has a finite geometric acceptance, which limits the fraction of pro-
 185 duced dimuon events that can be detected. This acceptance depends strongly on the event
 186 kinematics, primarily the dimuon invariant mass (M) and Feynman- x (x_F). The acceptance
 187 correction factor is determined using MC simulations.

188 The acceptance, $A(M, x_F)$, is defined as the ratio of the number of simulated events that
 189 are successfully reconstructed and pass all analysis cuts (N_{reco}) to the total number of events
 190 generated in a given kinematic bin (N_{gen}):

$$\text{Acceptance (A)} = \frac{N_{\text{reco}}}{N_{\text{gen}}} \quad (5)$$

191 This calculation is performed in bins of M and x_F . The kinematic binning used for this study
 192 is defined by the following edges:

- 193 • **x_F Edges:** $\{0, 0.05, 0.1, \dots, 0.8\}$ (16 bins)
 194 • **Mass Edges (GeV/c²):** $\{4.2, 4.5, 4.8, 5.1, 5.4, 5.7, 6, 6.3, 6.6, 6.9, 7.5, 8.7\}$ (11 bins)

195 The following pages show the calculated acceptance as a function of mass for each of the
 196 16 x_F bins. The plots show the acceptance for the LH₂ and LD₂ targets, their combined
 197 average, and their ratio. The ratio is close to unity across the kinematic range, indicating that
 198 target-dependent effects on the acceptance are small. In this case, we compare newly calculated
 199 acceptance corrections to the existing acceptance calculations saved in Shivangi's file:

200 `./shivangi/work/analysis/R008/diffCross/v42/5770/looseCut/final/acceptance_h.root`

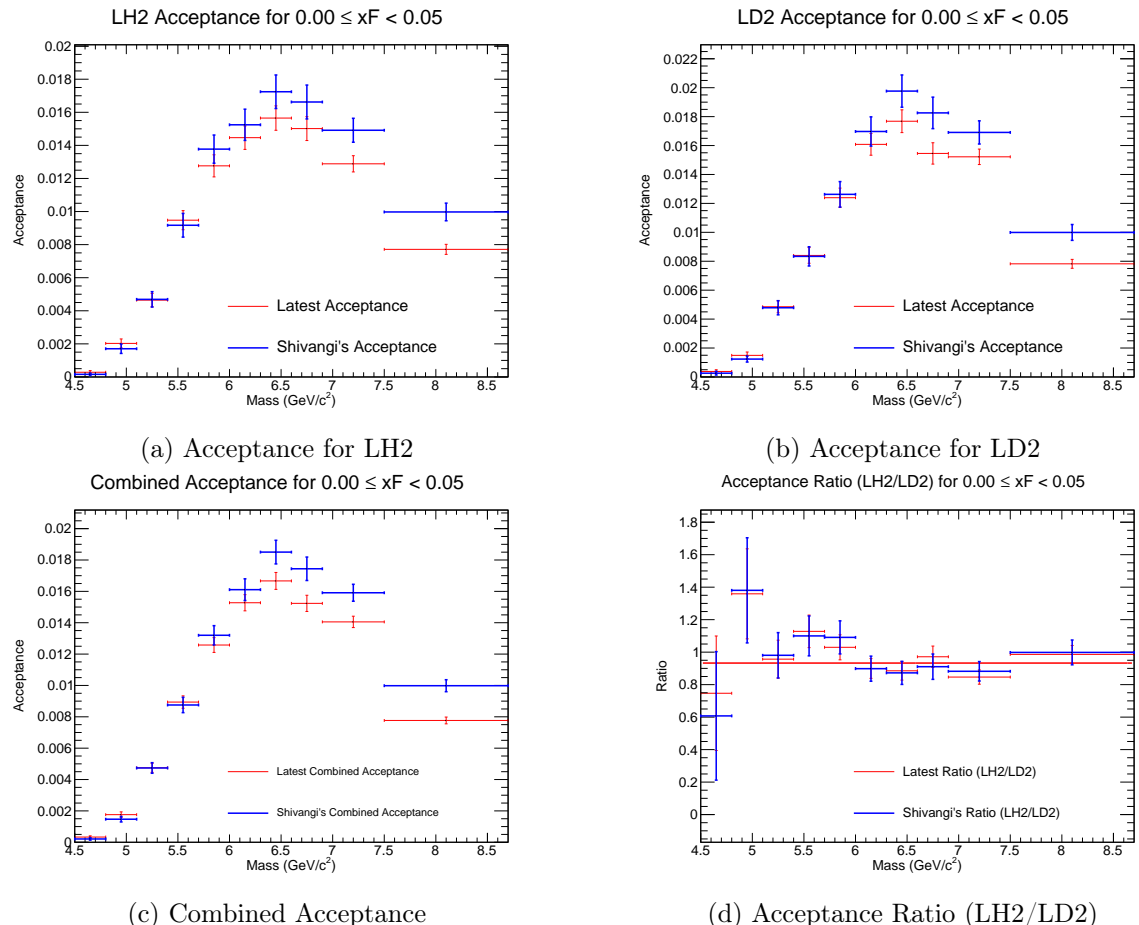


Figure 1: Acceptance plots for $0.00 \leq x_F < 0.05$.

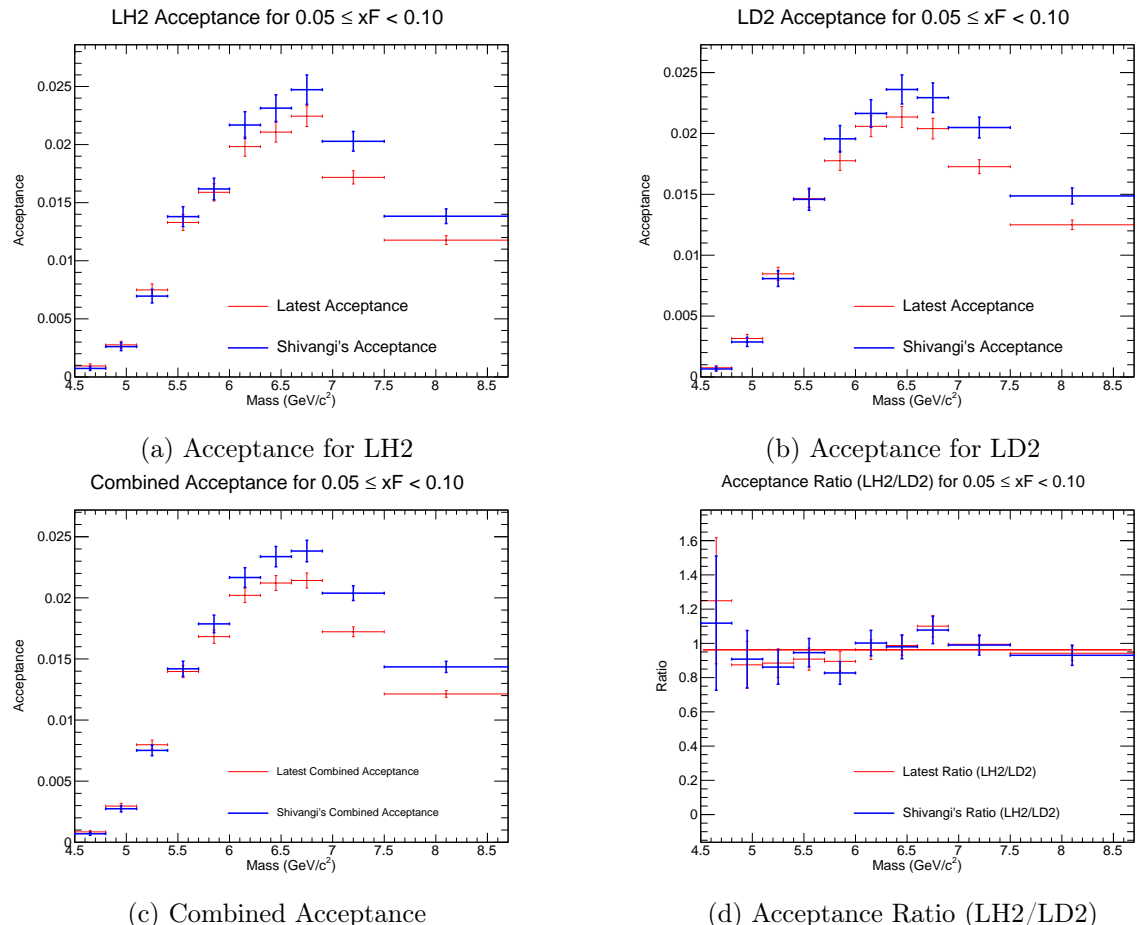


Figure 2: Acceptance plots for $0.05 \leq x_F < 0.10$.

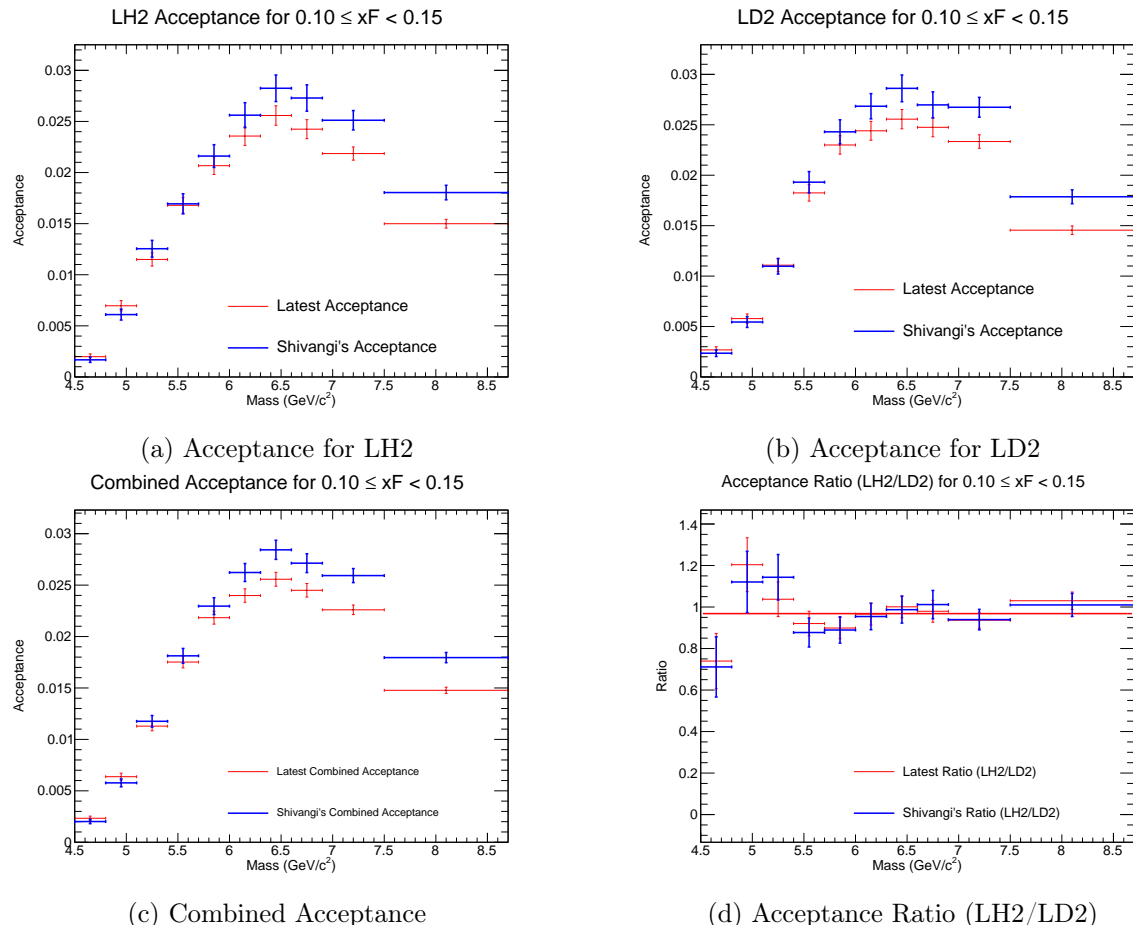


Figure 3: Acceptance plots for $0.10 \leq x_F < 0.15$.

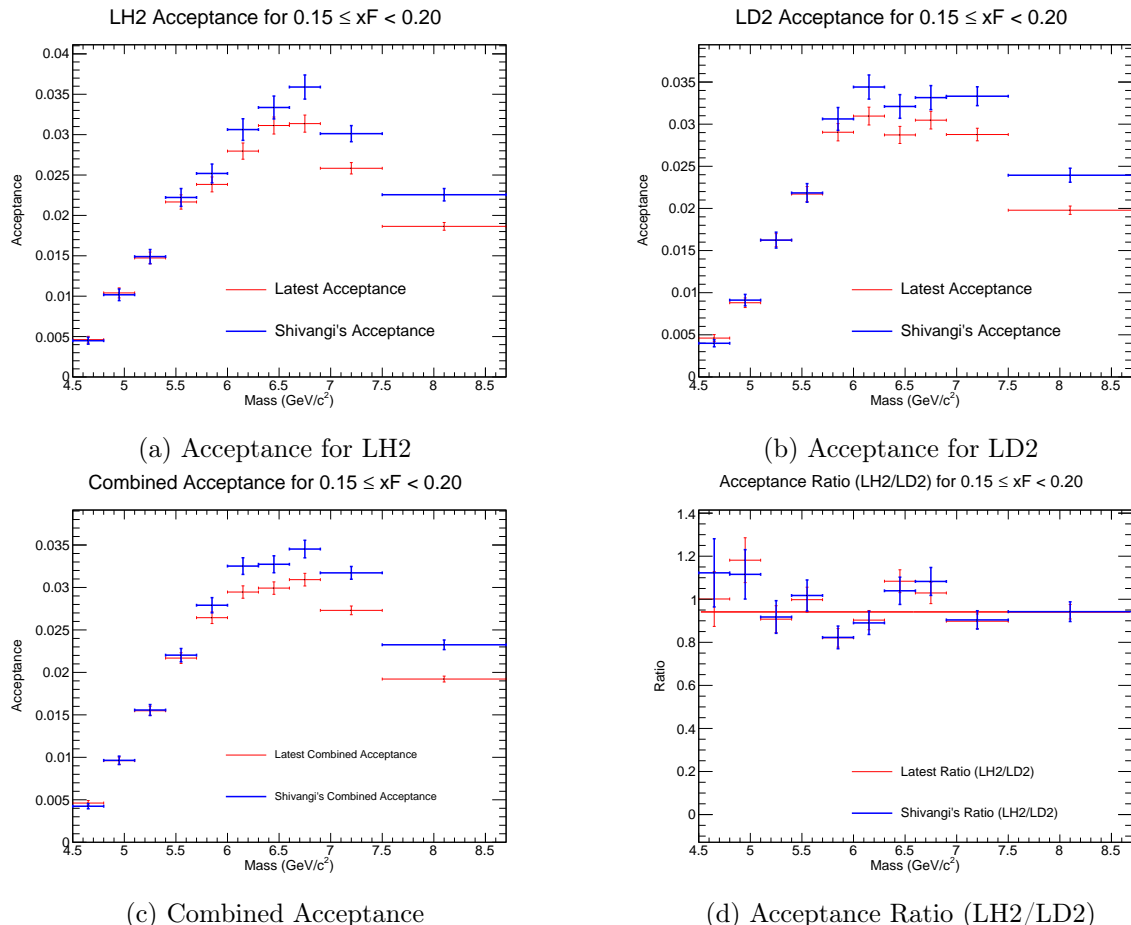


Figure 4: Acceptance plots for $0.15 \leq x_F < 0.20$.

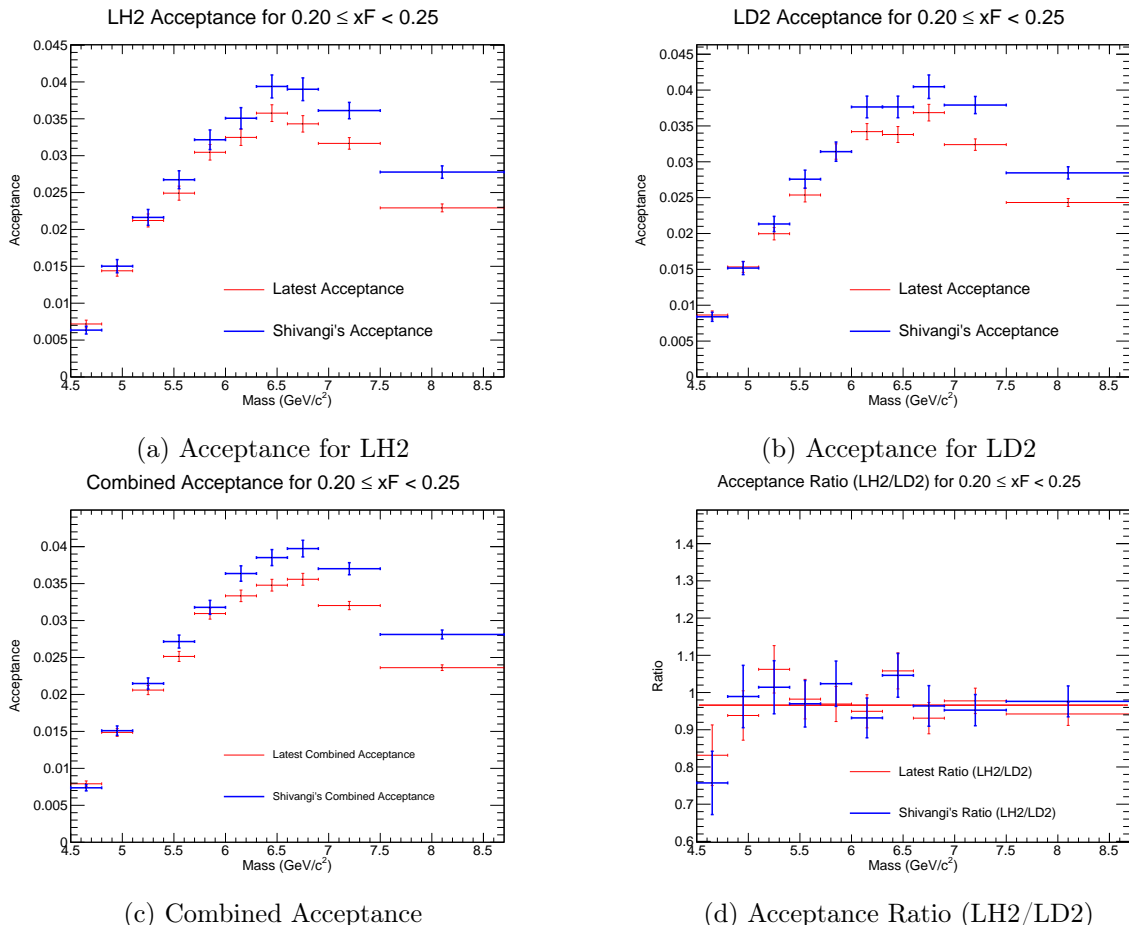


Figure 5: Acceptance plots for $0.20 \leq x_F < 0.25$.

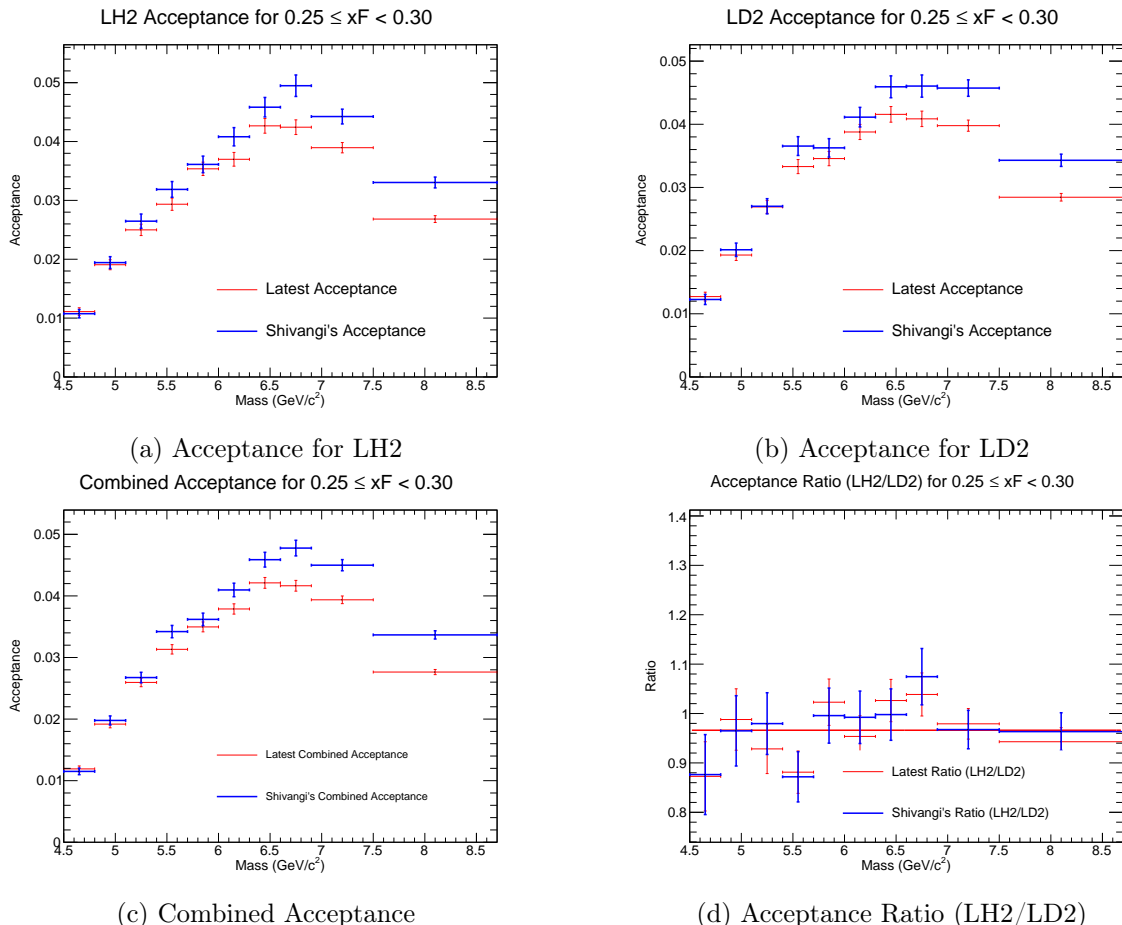


Figure 6: Acceptance plots for $0.25 \leq x_F < 0.30$.

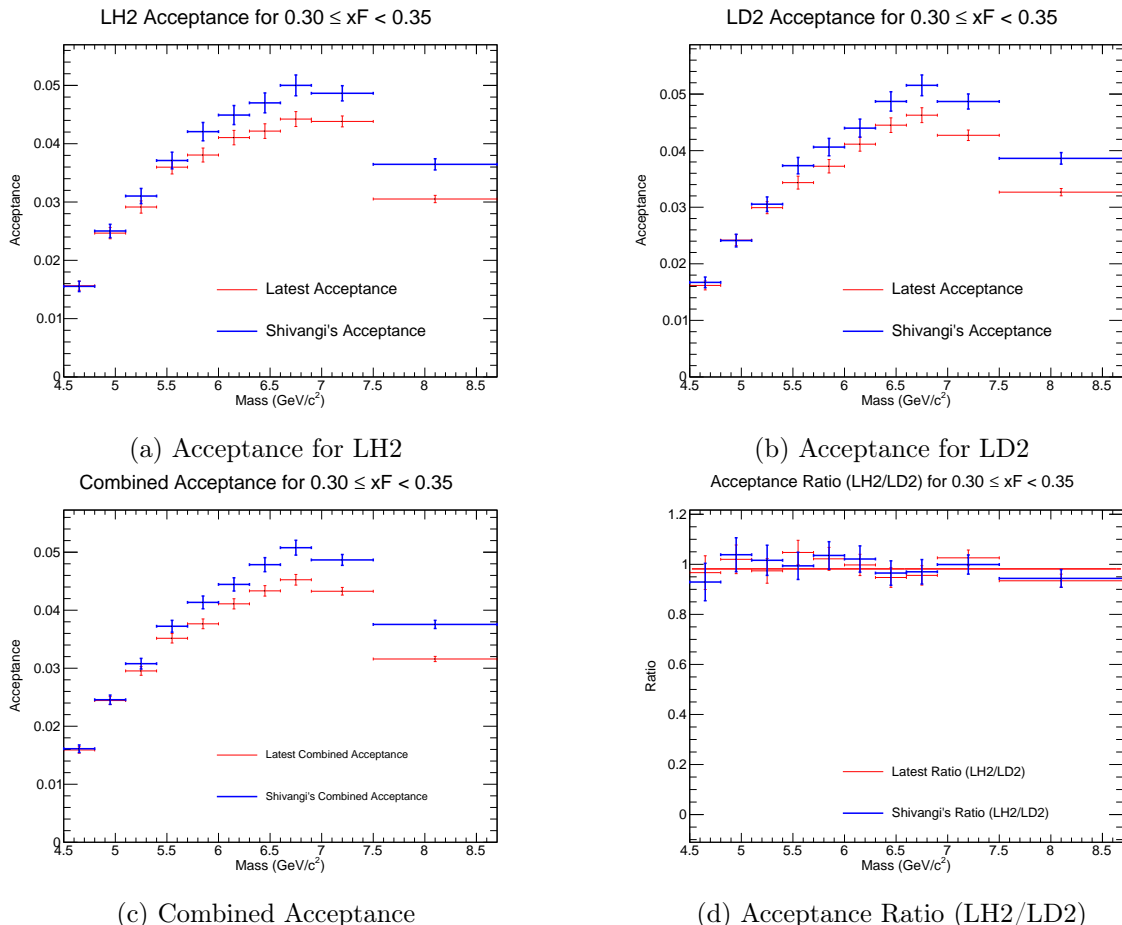


Figure 7: Acceptance plots for $0.30 \leq x_F < 0.35$.

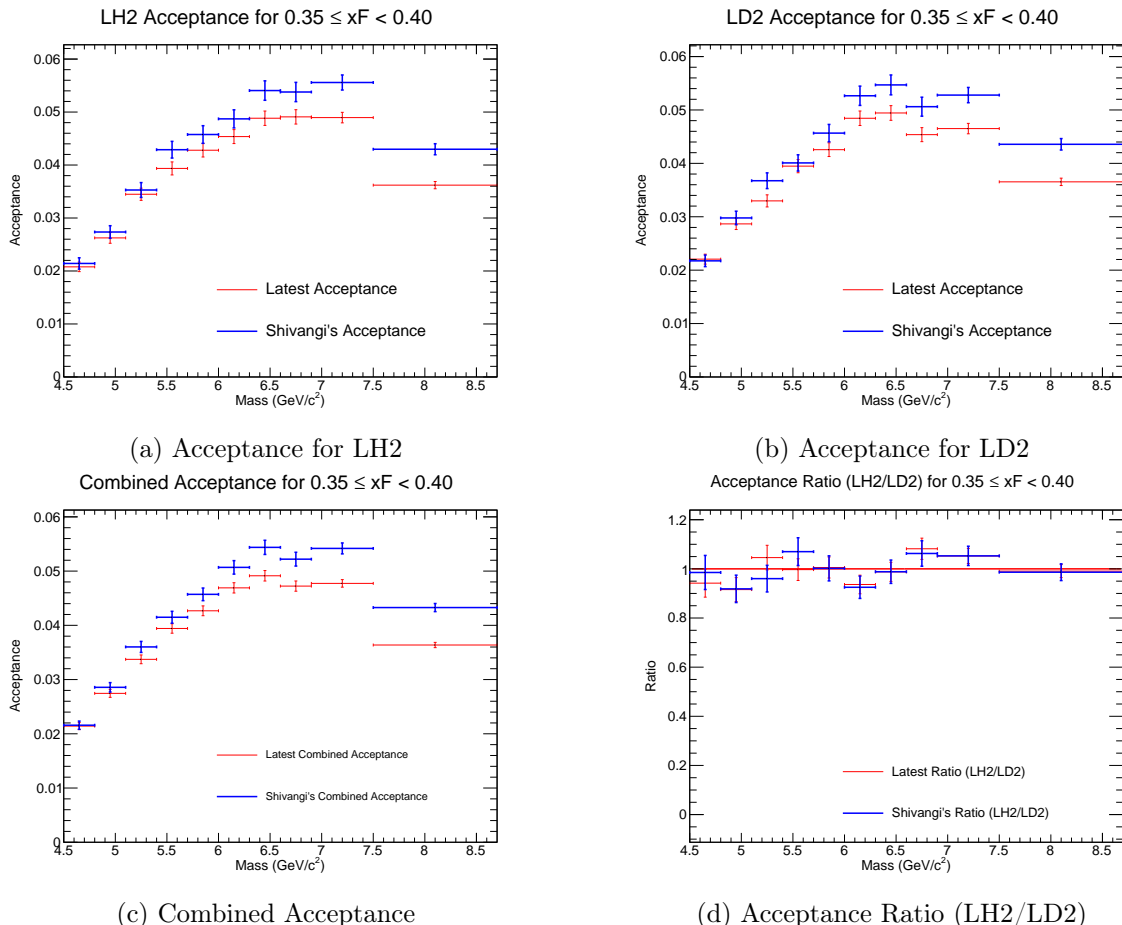


Figure 8: Acceptance plots for $0.35 \leq x_F < 0.40$.

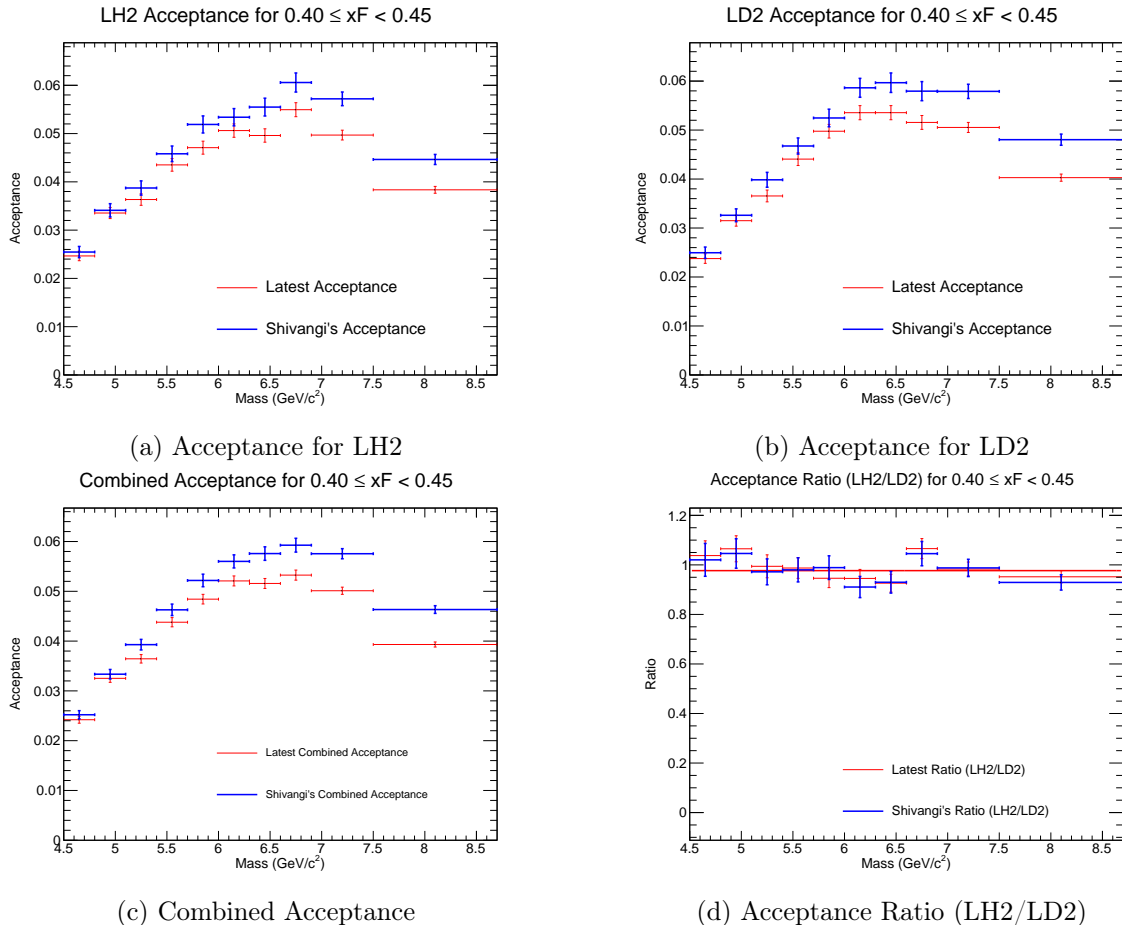


Figure 9: Acceptance plots for $0.40 \leq x_F < 0.45$.

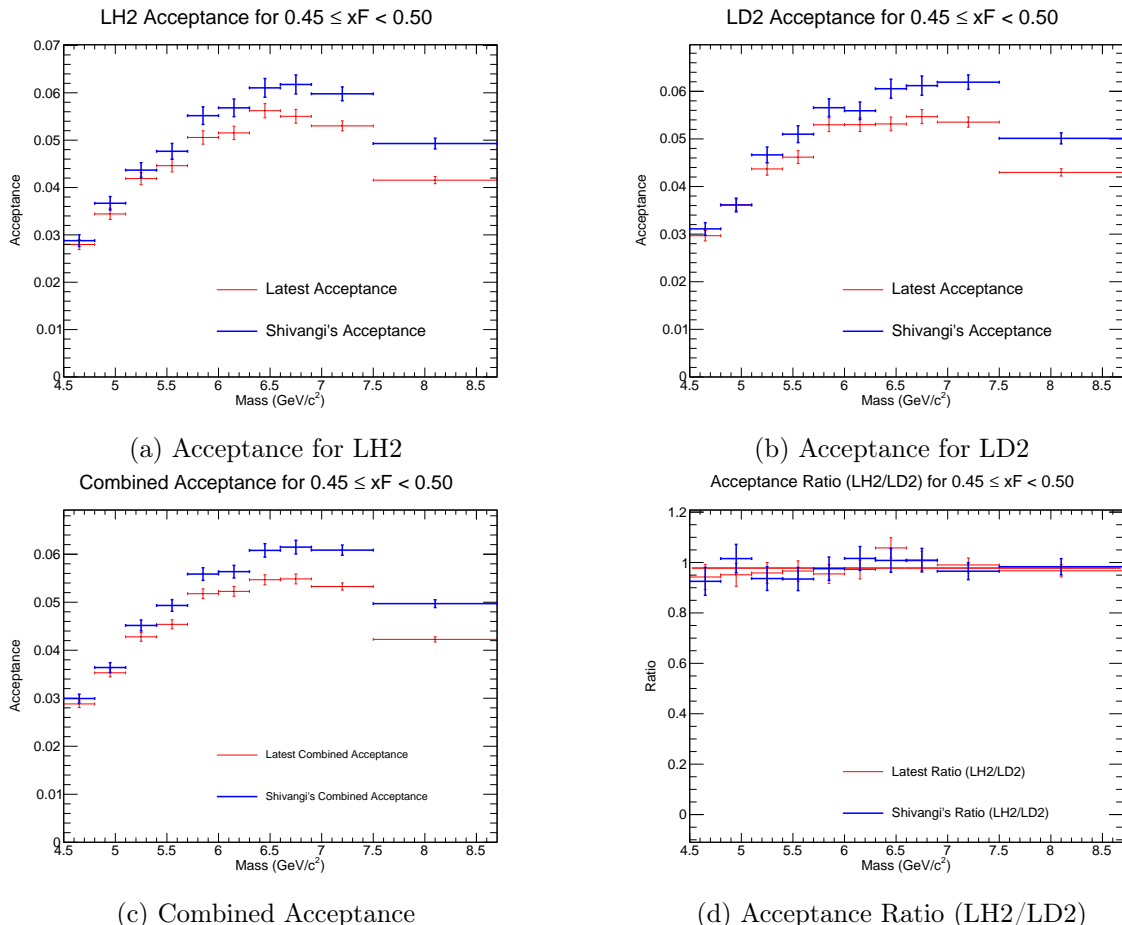


Figure 10: Acceptance plots for $0.45 \leq x_F < 0.50$.

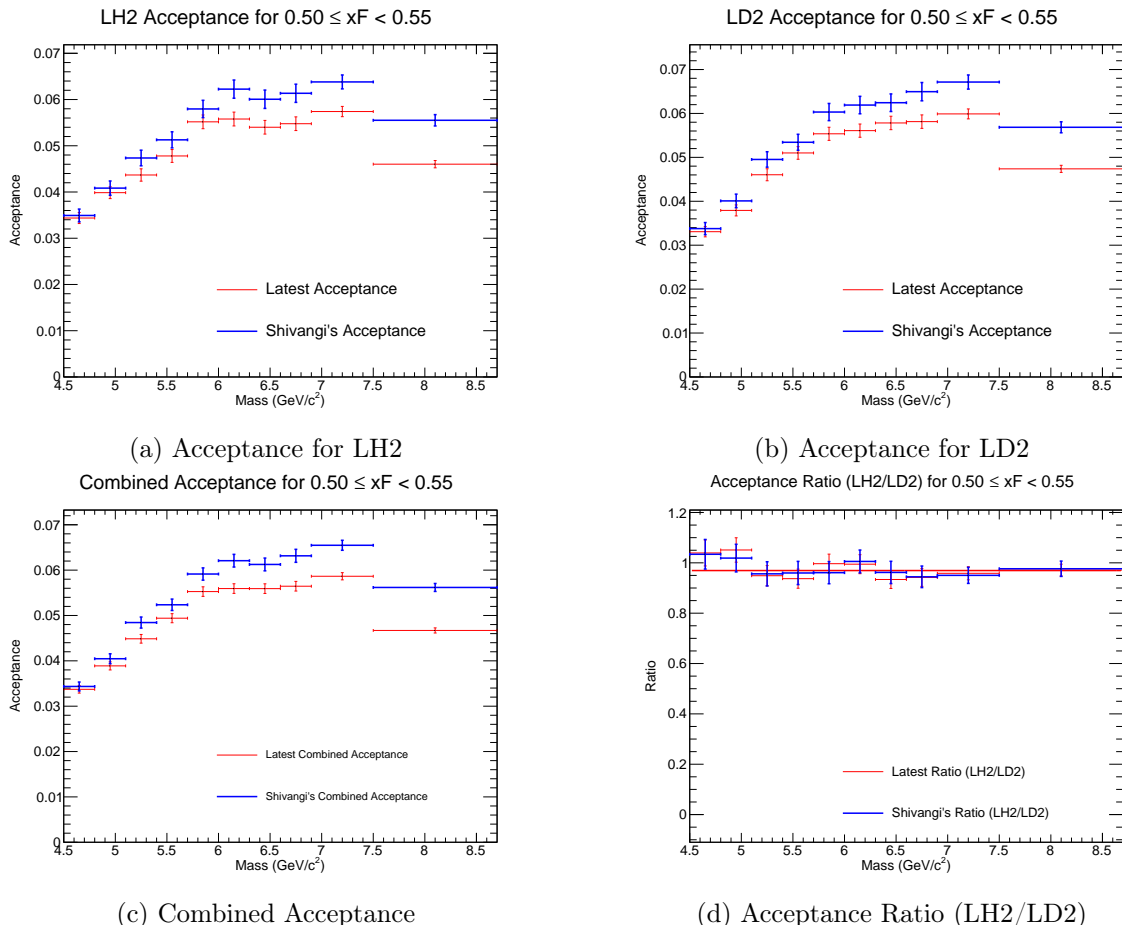


Figure 11: Acceptance plots for $0.50 \leq x_F < 0.55$.

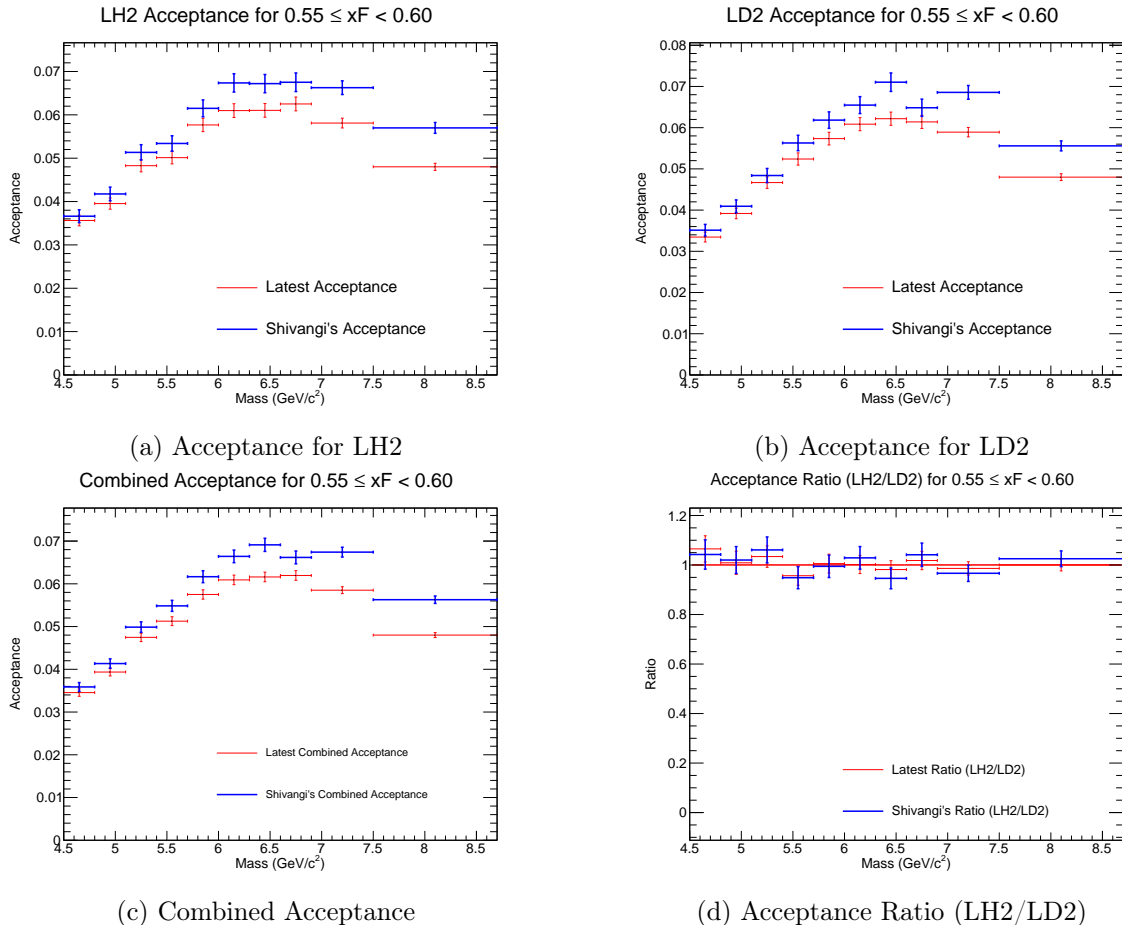


Figure 12: Acceptance plots for $0.55 \leq x_F < 0.60$.

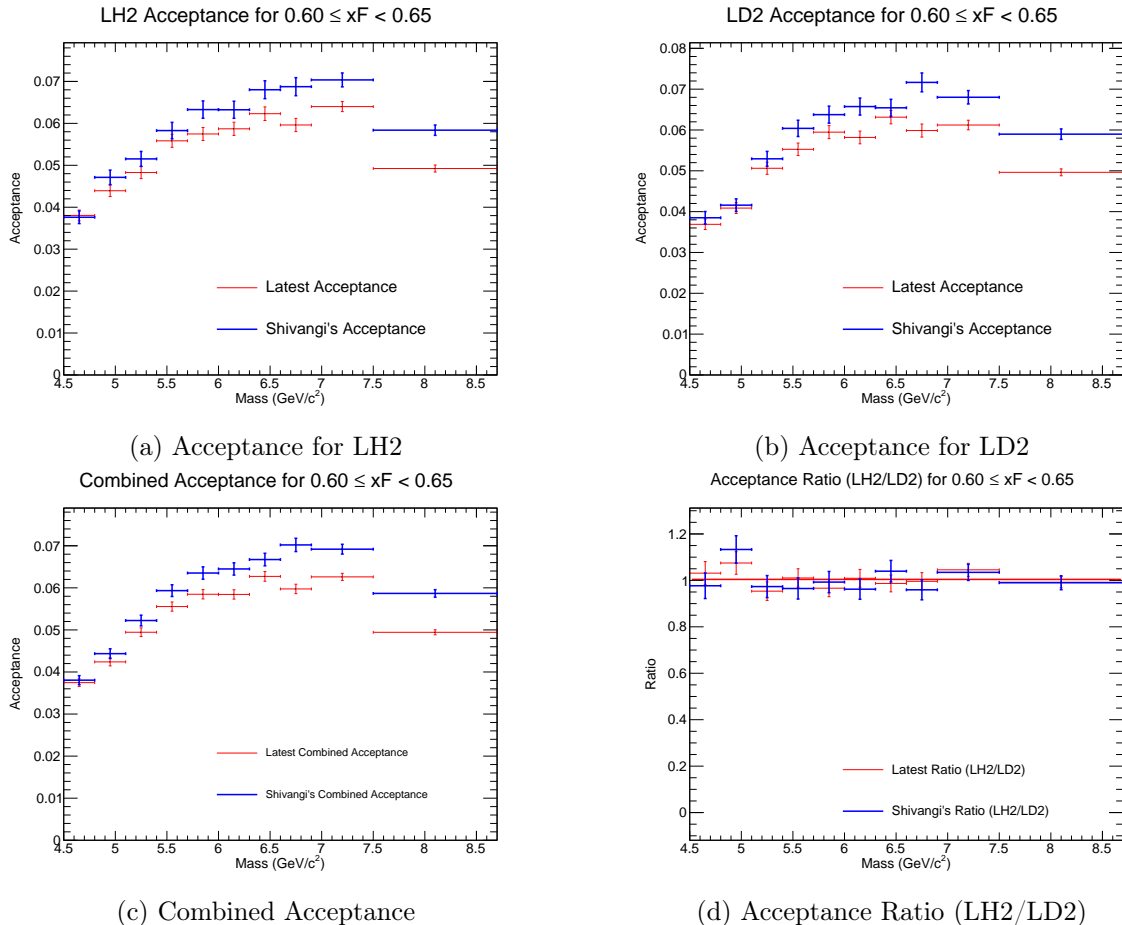


Figure 13: Acceptance plots for $0.60 \leq x_F < 0.65$.

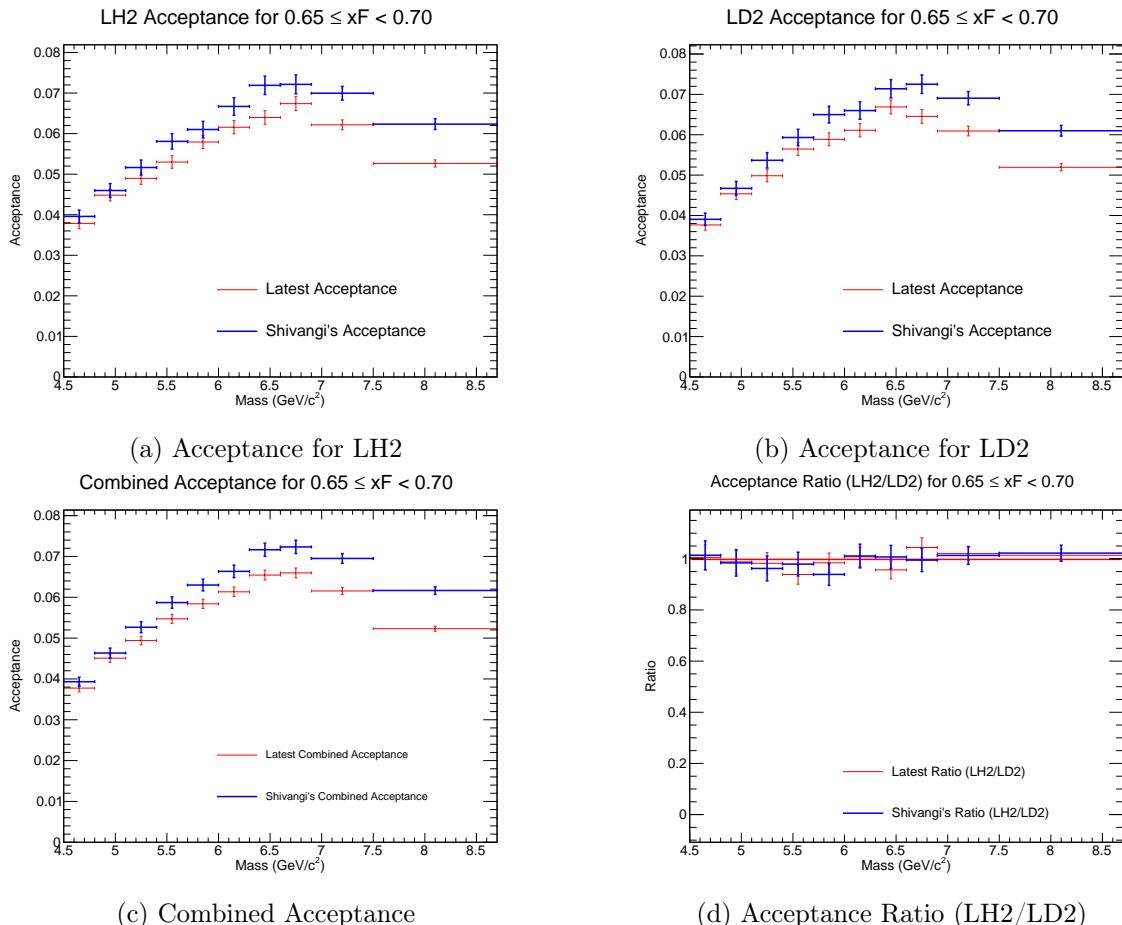


Figure 14: Acceptance plots for $0.65 \leq x_F < 0.70$.

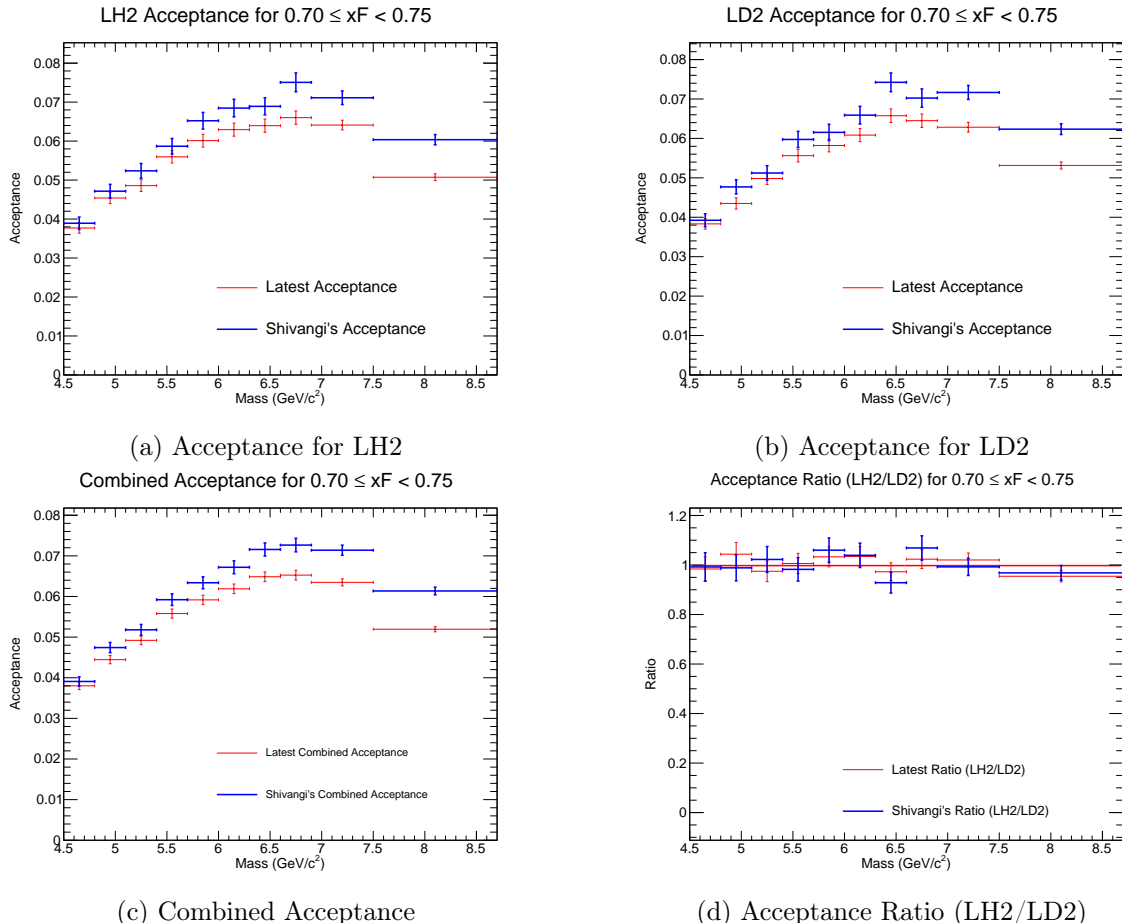


Figure 15: Acceptance plots for $0.70 \leq x_F < 0.75$.

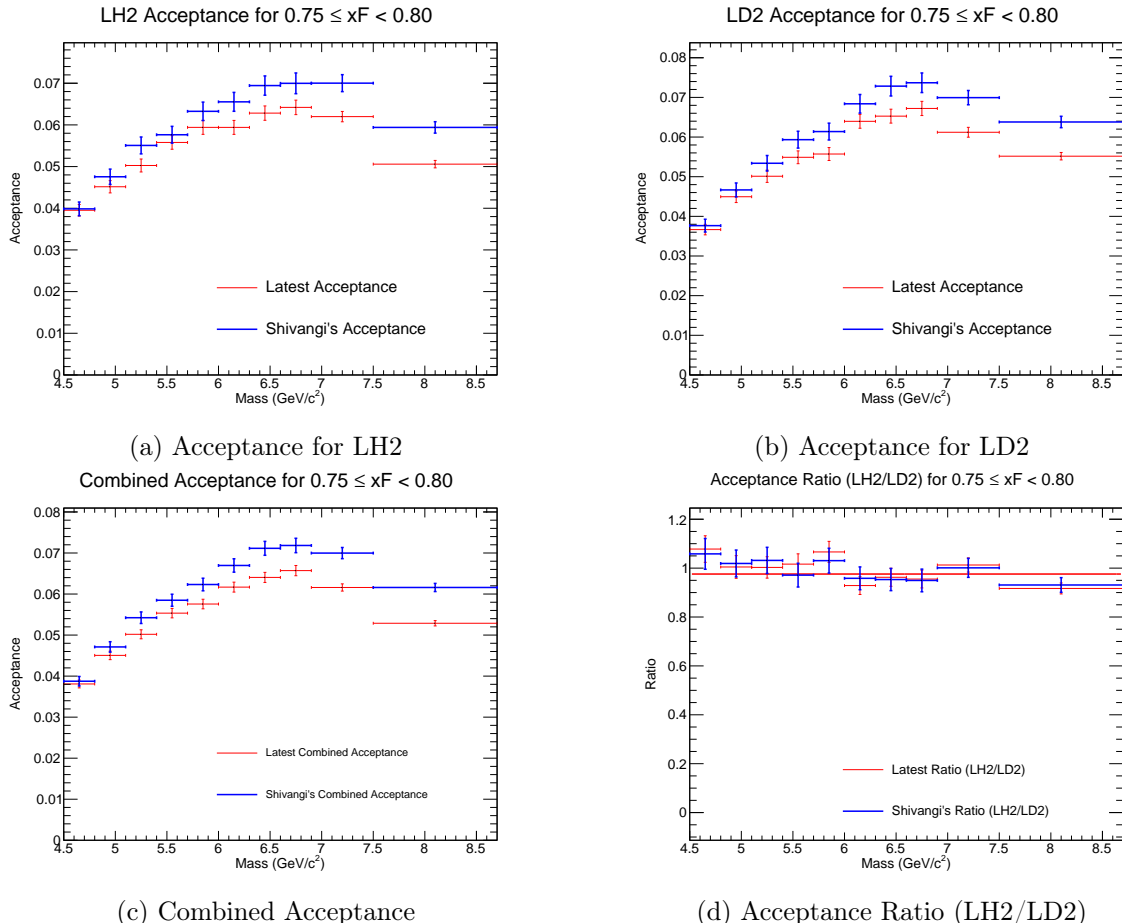


Figure 16: Acceptance plots for $0.75 \leq x_F < 0.80$.

201 **3.2 Reconstruction Efficiency Correction**

202 The track-finding algorithm ("kTracker") has an efficiency that depends on the detector oc-
 203 cupancy; the number of hits from unrelated particles in the detector during an event. This
 204 efficiency is studied using "clean" MC simulations (signal only) and "messy" MC simulations
 205 (signal with background hits overlaid). The reconstruction efficiency, ϵ_{recon} , is defined as the
 206 ratio of events found in the messy sample to those in the clean sample, as a function of an
 207 occupancy-related variable (e.g., D2, the number of hits in Drift Chamber Station 2).

$$\epsilon_{\text{recon}}(\text{D2}, M, x_F) = \frac{N_{\text{reco}}^{\text{messy}}(\text{D2}, M, x_F)}{N_{\text{reco}}^{\text{clean}}(M, x_F)} \quad (6)$$

208 For each kinematic bin of (M, x_F) , an efficiency curve as a function of D2 is generated from
 209 the MC. To obtain a single correction factor for each bin, an average efficiency, $\langle \epsilon \rangle$, is calculated
 210 by weighting this efficiency curve by the D2 distribution of the experimental data in that same
 211 bin.

212 **3.2.1 Uncertainty Propagation**

213 An important aspect of this procedure is the correct propagation of uncertainties. For each event
 214 in the data with a measured D2 value, an efficiency ϵ_i and its uncertainty $\delta\epsilon_i$ are determined by
 215 linear interpolation between points on the MC-derived efficiency curve.

216 The average efficiency $\langle \epsilon \rangle$ for a bin containing N data events is the mean of the individual
 217 efficiencies:

$$\langle \epsilon \rangle = \frac{1}{N} \sum_{i=1}^N \epsilon_i \quad (7)$$

218 The uncertainty on this average, $\delta\langle \epsilon \rangle$, has two components: a statistical error from the spread
 219 of efficiencies within the data distribution, and a propagated error from the uncertainty on the
 220 MC-derived efficiency curve itself. The latter is the dominant systematic uncertainty for this
 221 correction and is calculated as:

$$\delta_{\text{prop}}\langle \epsilon \rangle = \frac{1}{N} \sqrt{\sum_{i=1}^N (\delta\epsilon_i)^2} \quad (8)$$

222 The final correction applied to the data is $1/\langle \epsilon \rangle$, and its propagated error is given by:

$$\delta(1/\langle \epsilon \rangle) = \frac{\delta_{\text{prop}}\langle \epsilon \rangle}{\langle \epsilon \rangle^2} \quad (9)$$

223 **3.2.2 Efficiency Results**

224 The efficiency curves as a function of D2 were generated for all kinematic bins. The following
 225 pages display these curves, with each page corresponding to a single bin in x_F , showing the
 226 results for all 11 mass bins. **It is clear that some bins have insufficient statistics, and**
 227 **we should perform additional MC simulation in the near future to remedy this.**

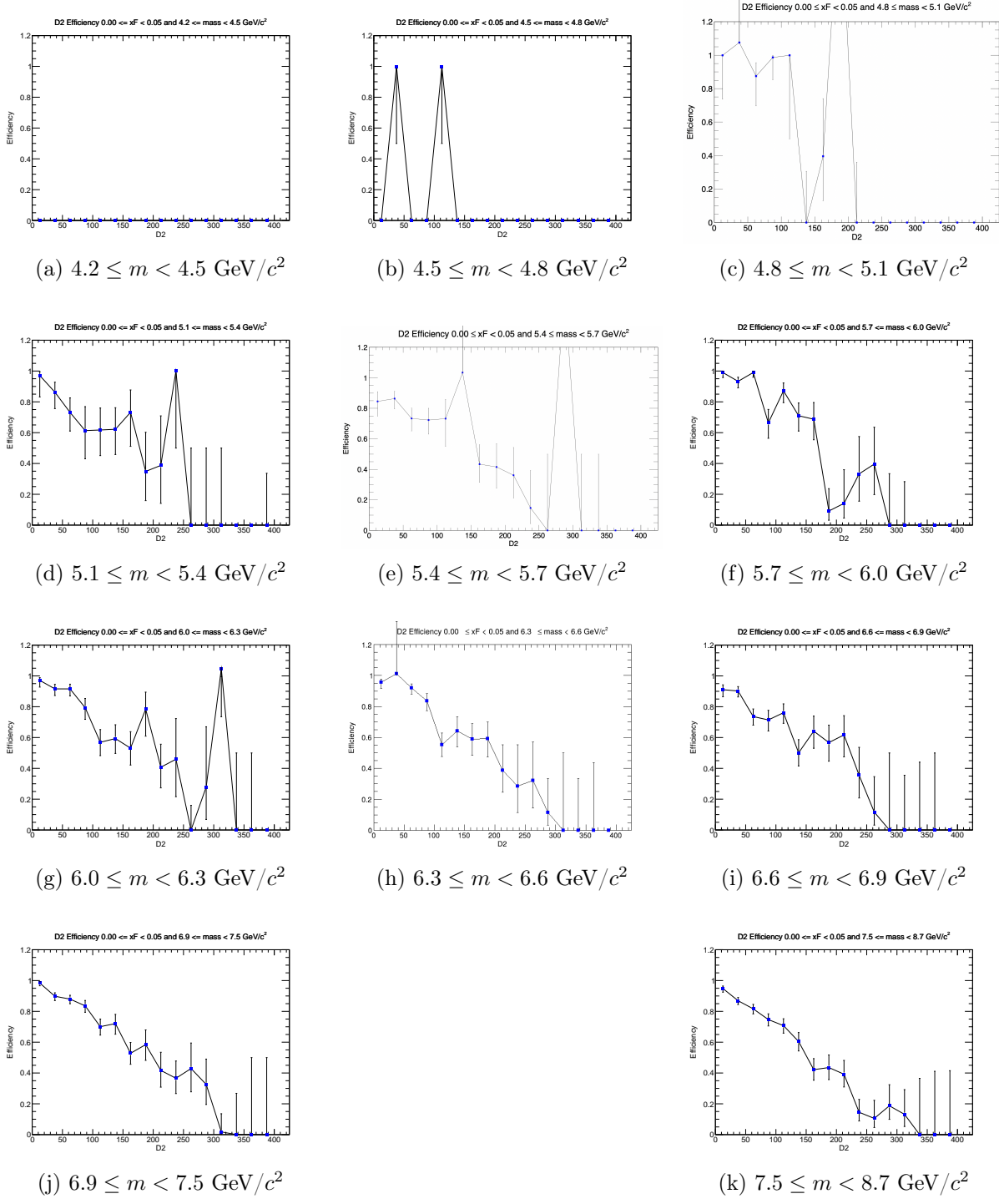


Figure 17: Efficiency plots for the x_F bin $0.00 \leq x_F < 0.05$.

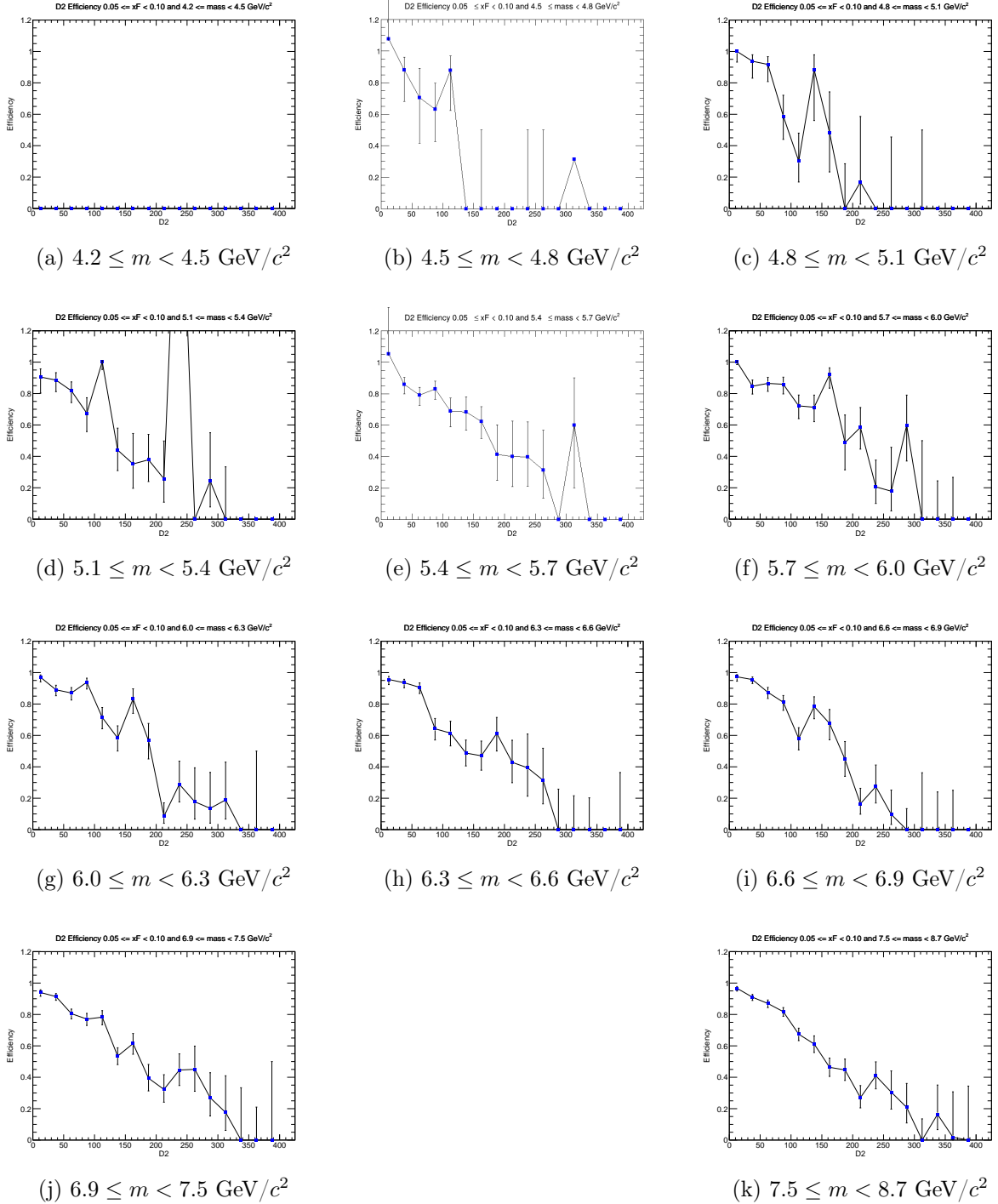


Figure 18: Efficiency plots for the x_F bin $0.05 \leq x_F < 0.10$.

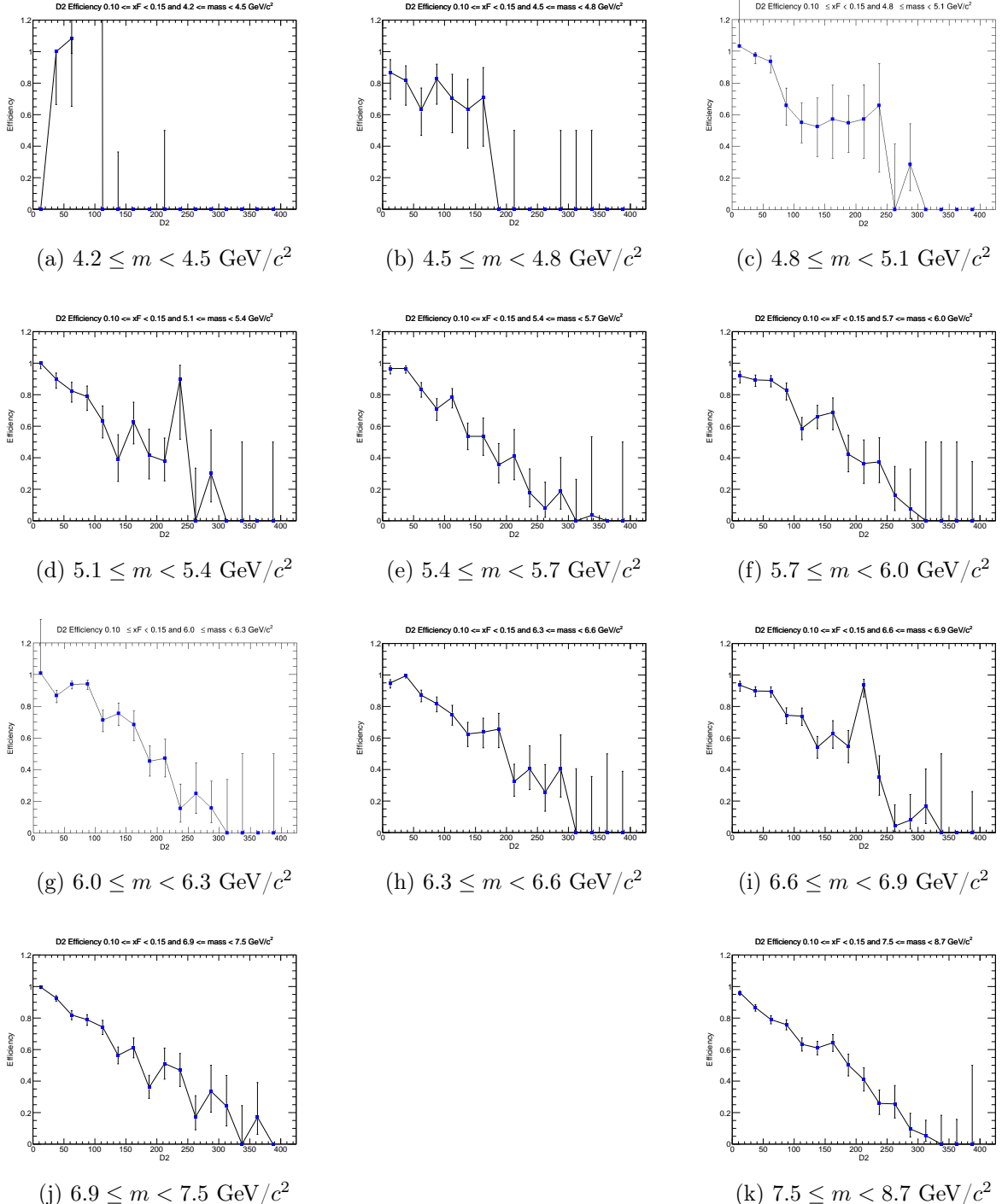


Figure 19: Efficiency plots for the x_F bin $0.10 \leq x_F < 0.15$.

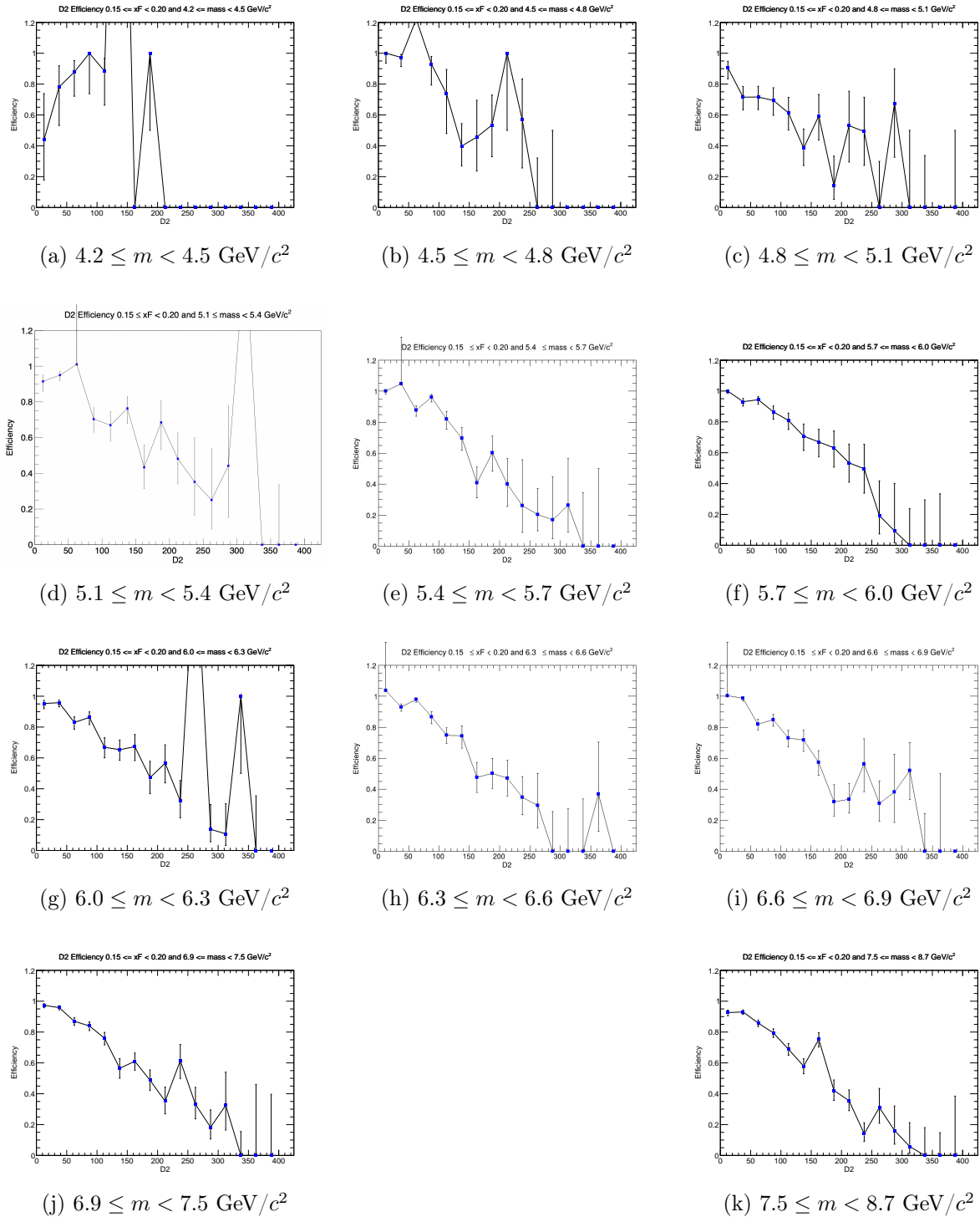


Figure 20: Efficiency plots for the x_F bin $0.15 \leq x_F < 0.20$.

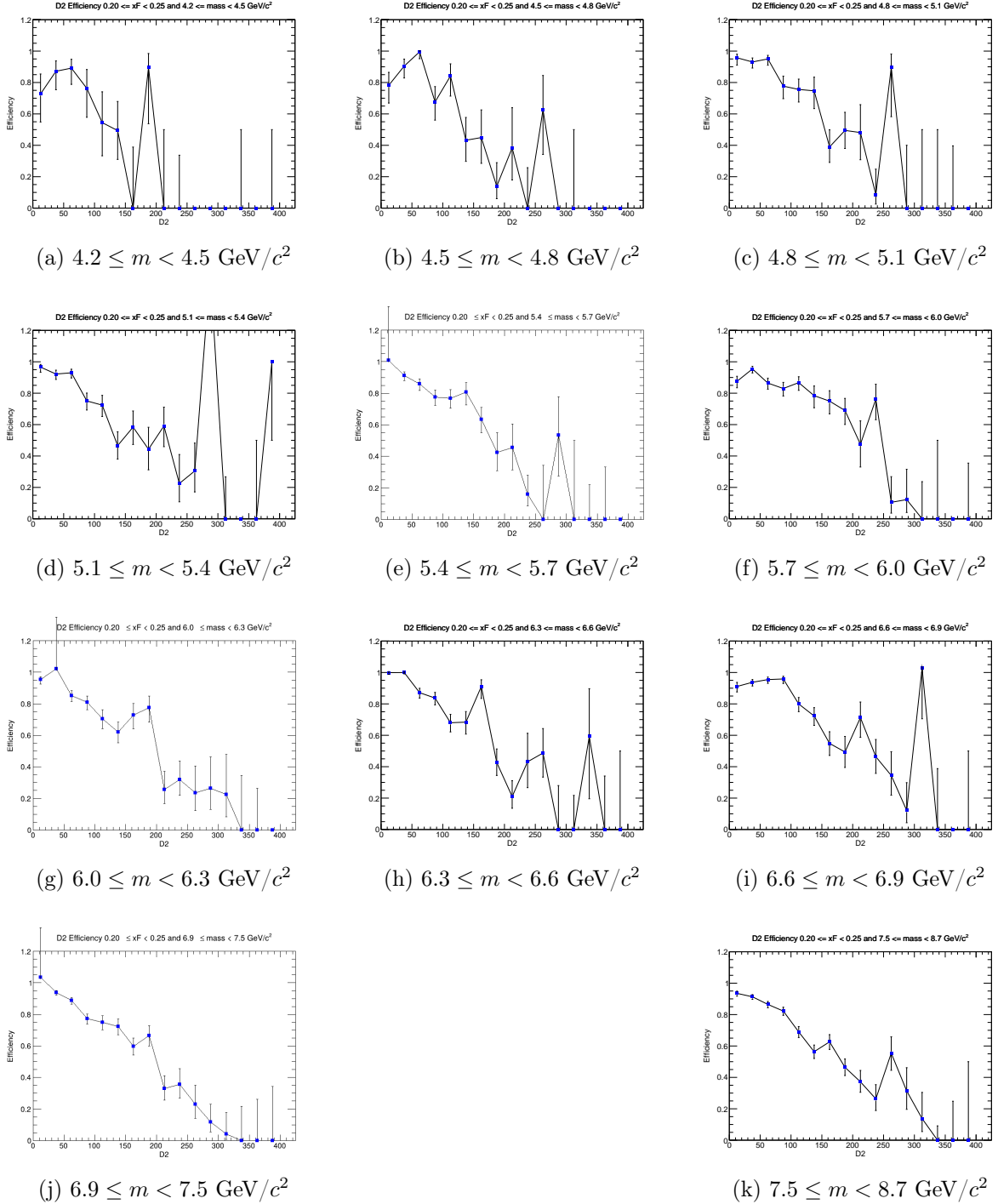


Figure 21: Efficiency plots for the x_F bin $0.20 \leq x_F < 0.25$.

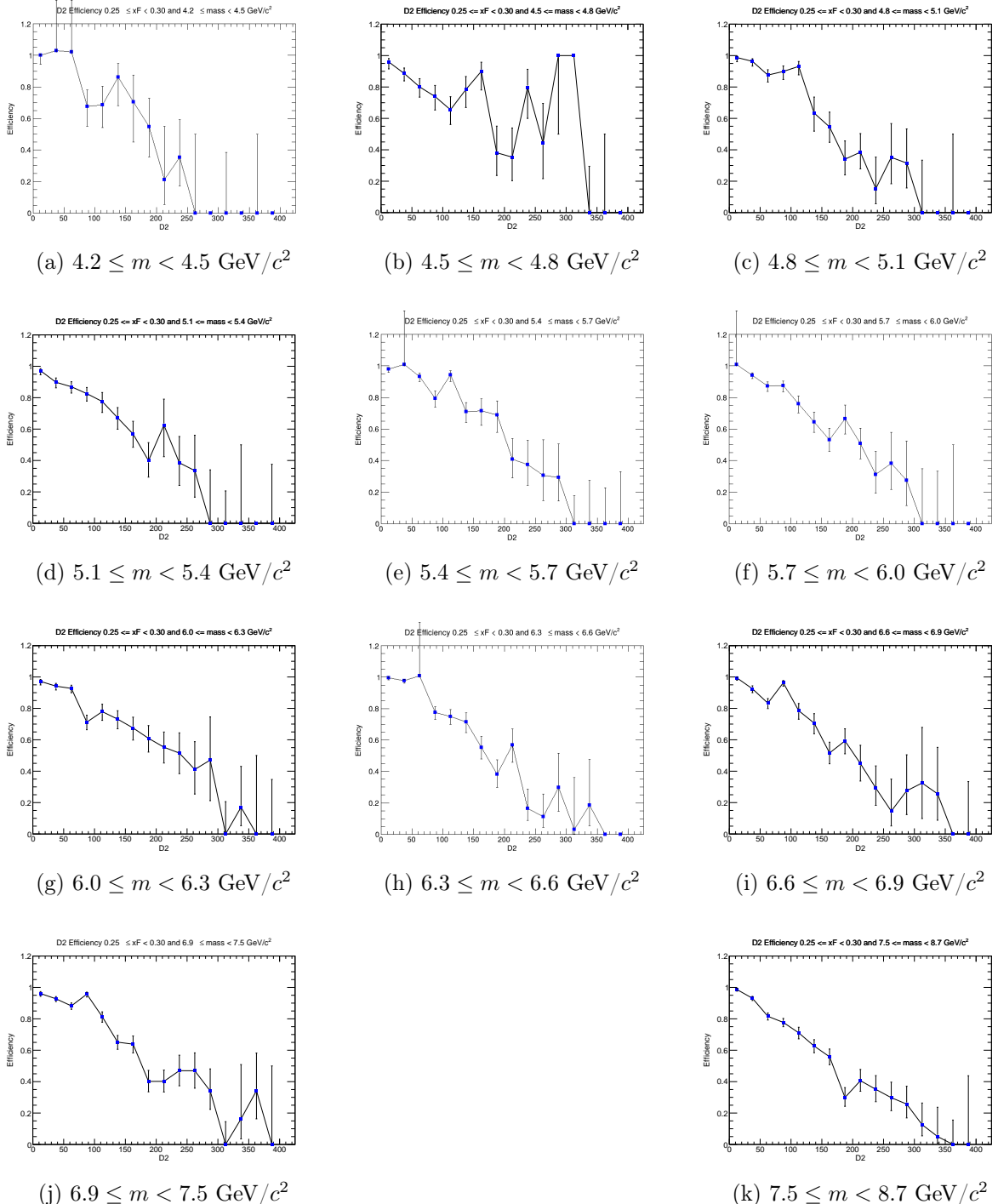


Figure 22: Efficiency plots for the x_F bin $0.25 \leq x_F < 0.30$.

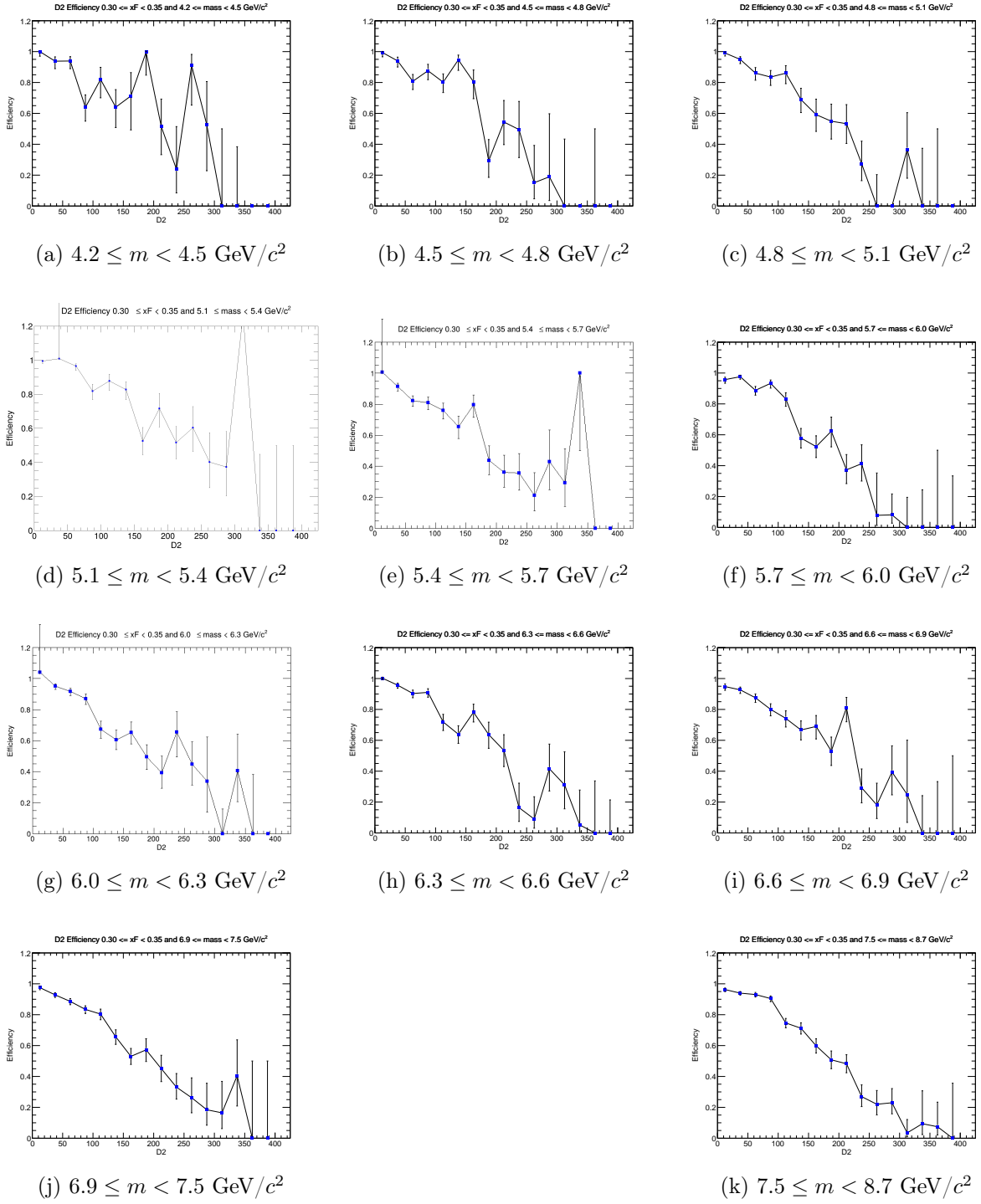


Figure 23: Efficiency plots for the x_F bin $0.30 \leq x_F < 0.35$.

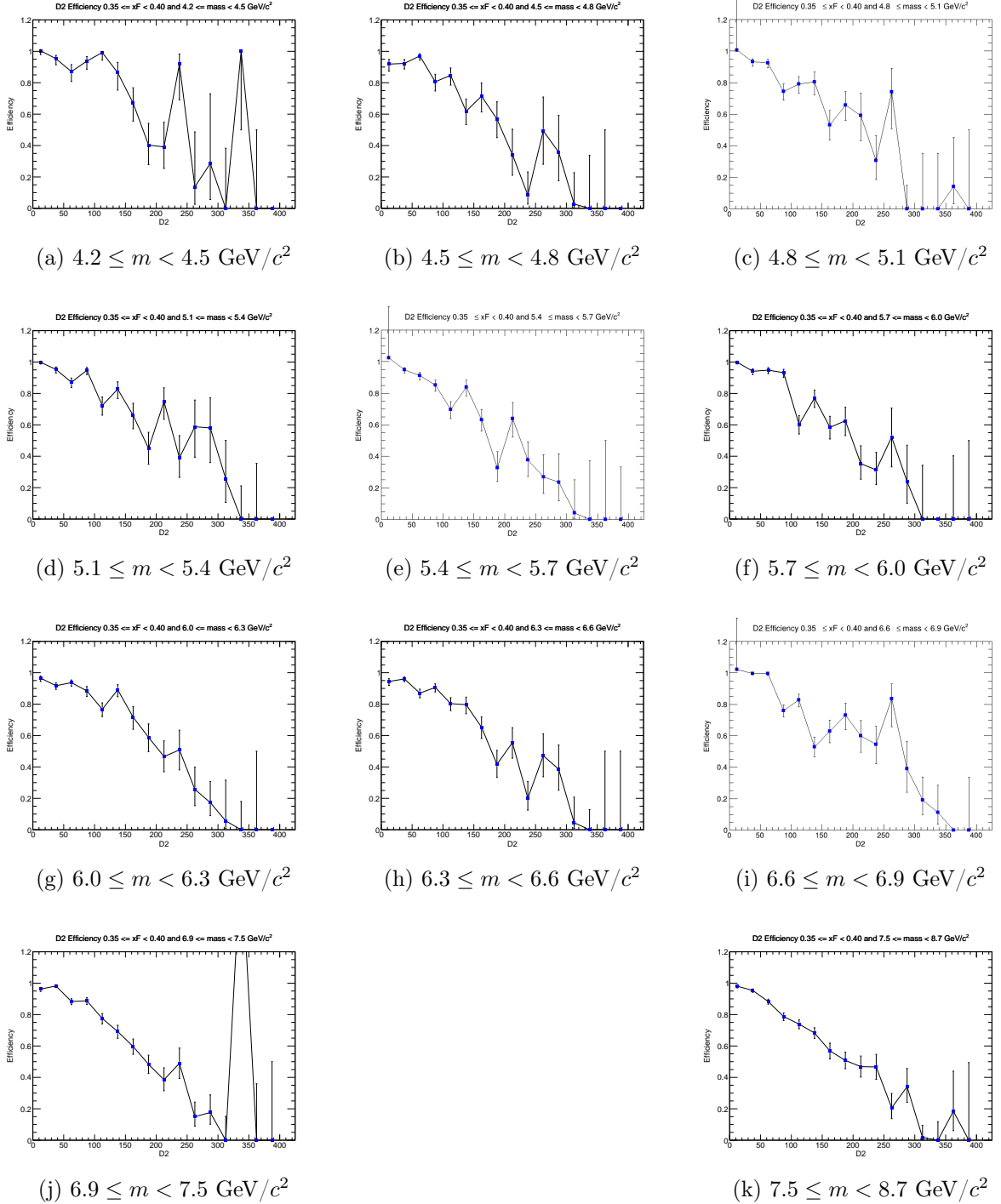


Figure 24: Efficiency plots for the x_F bin $0.35 \leq x_F < 0.40$.

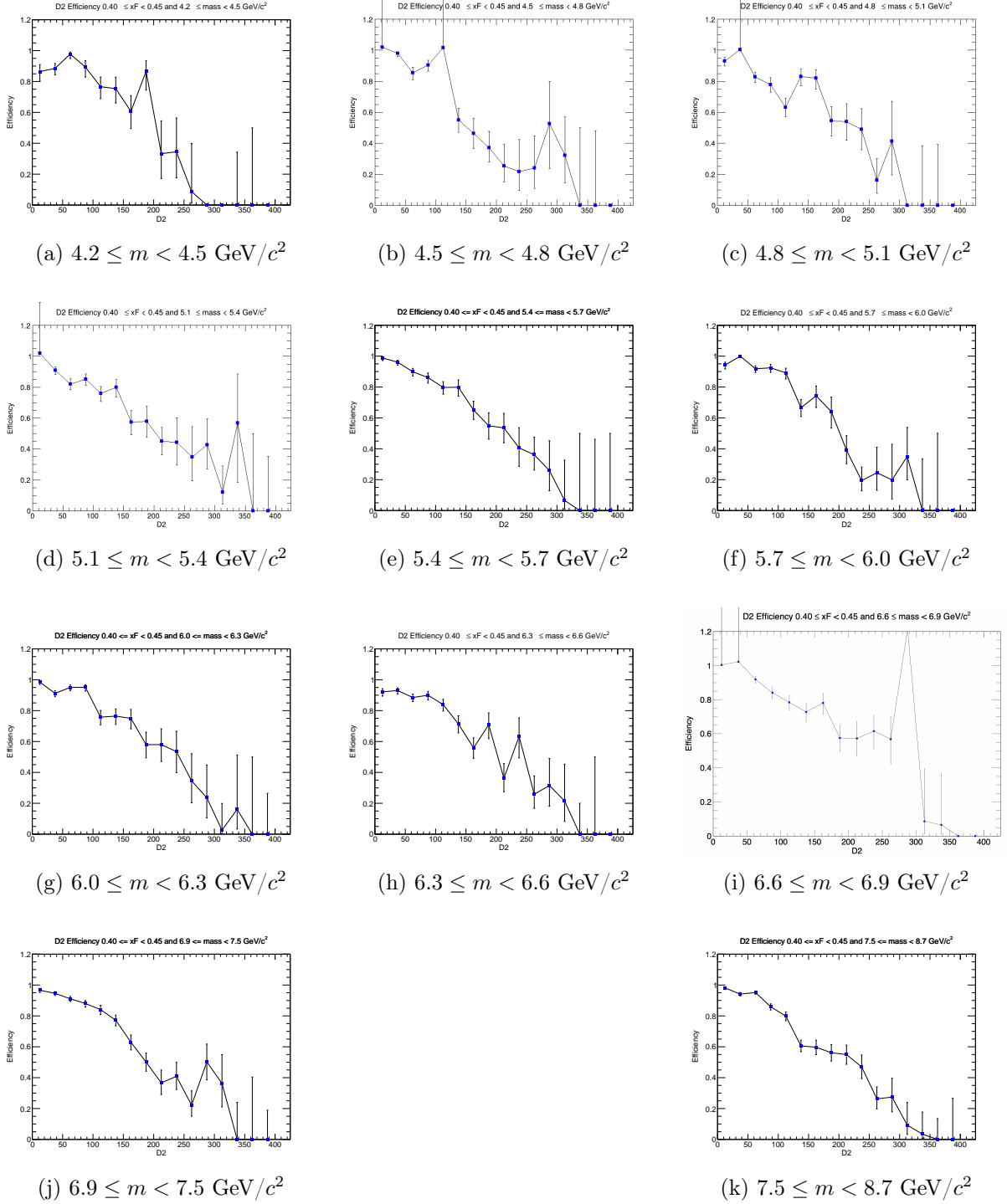


Figure 25: Efficiency plots for the x_F bin $0.40 \leq x_F < 0.45$.

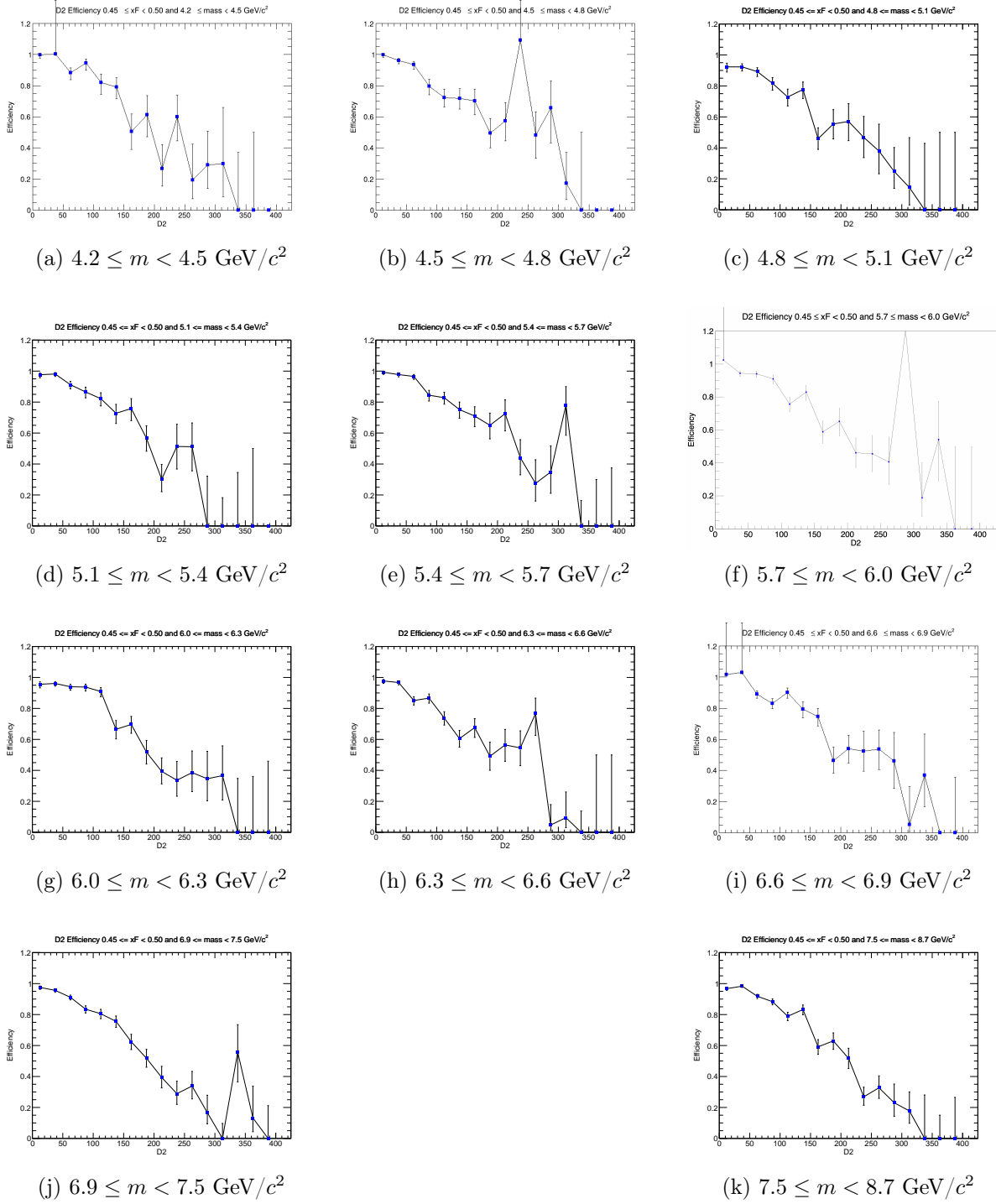


Figure 26: Efficiency plots for the x_F bin $0.45 \leq x_F < 0.50$.

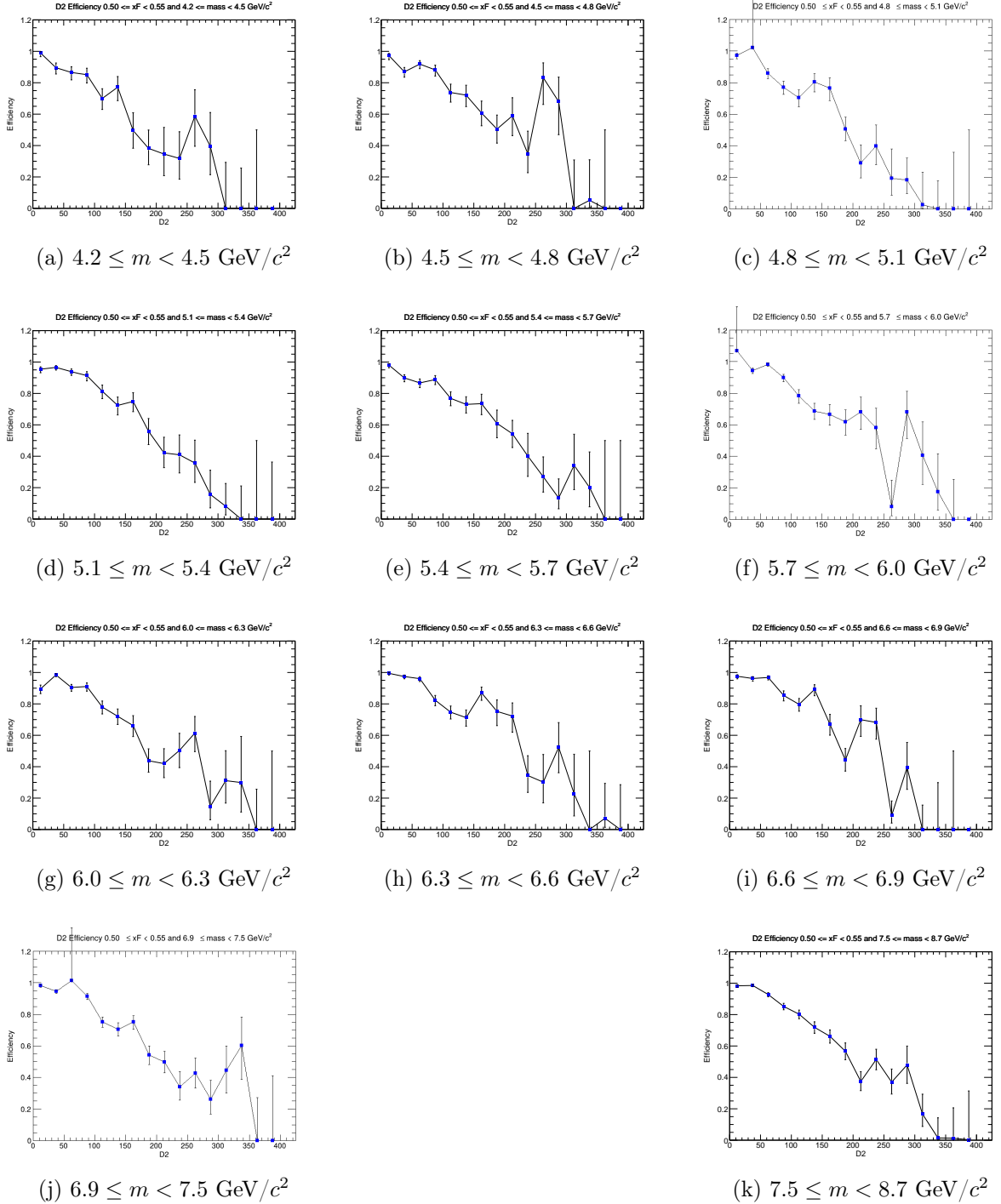


Figure 27: Efficiency plots for the x_F bin $0.50 \leq x_F < 0.55$.

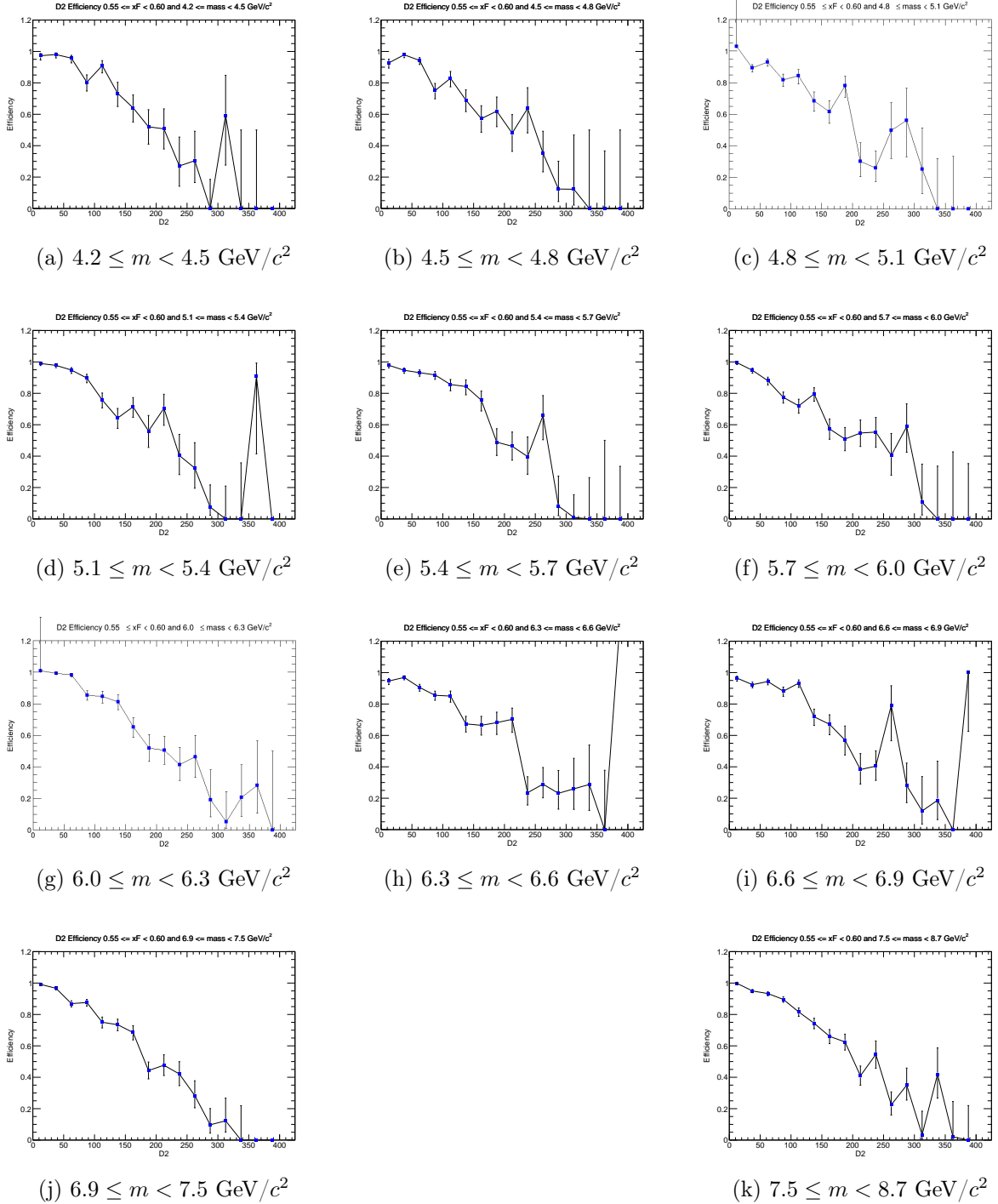


Figure 28: Efficiency plots for the x_F bin $0.55 \leq x_F < 0.60$.

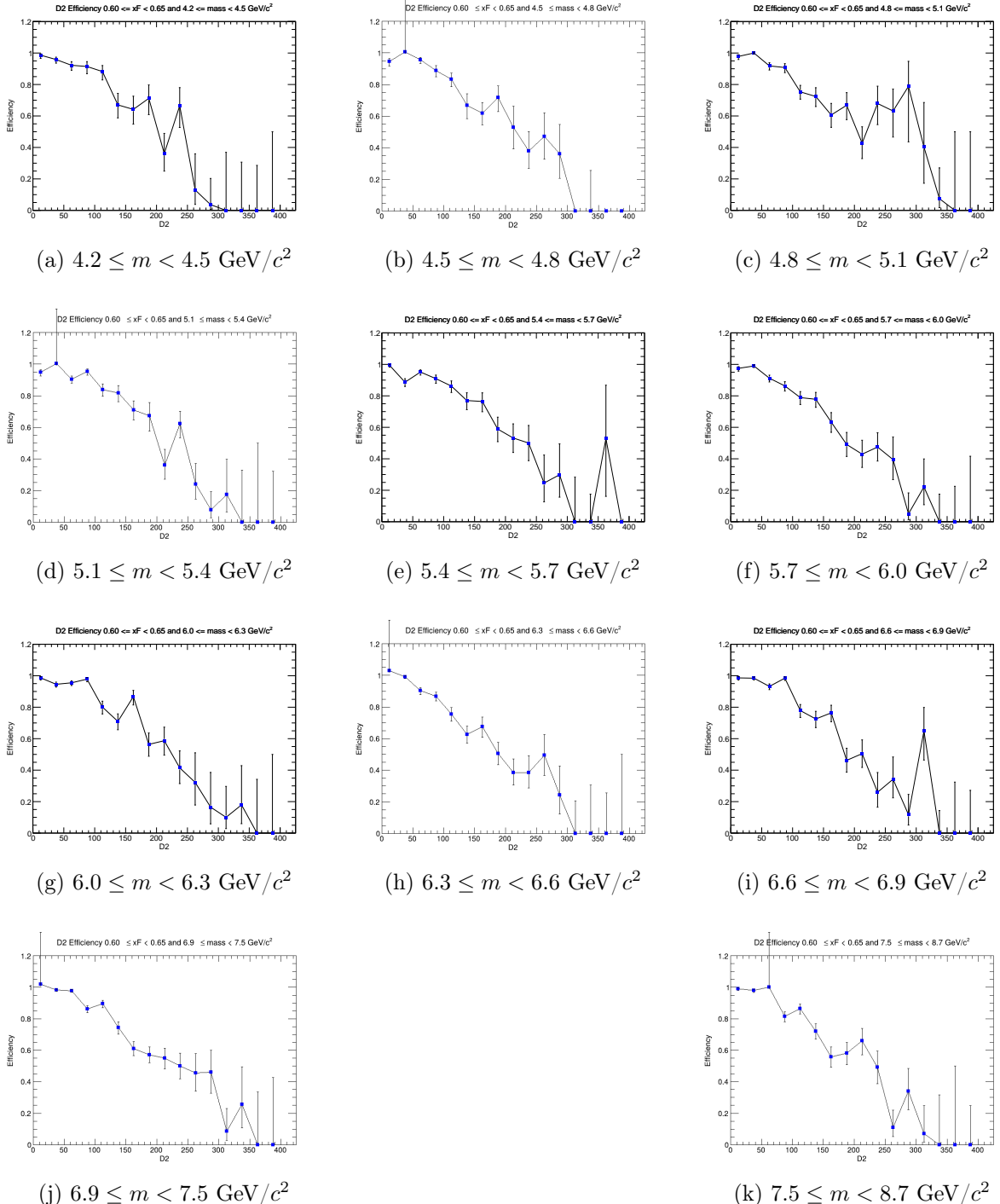


Figure 29: Efficiency plots for the x_F bin $0.60 \leq x_F < 0.65$.

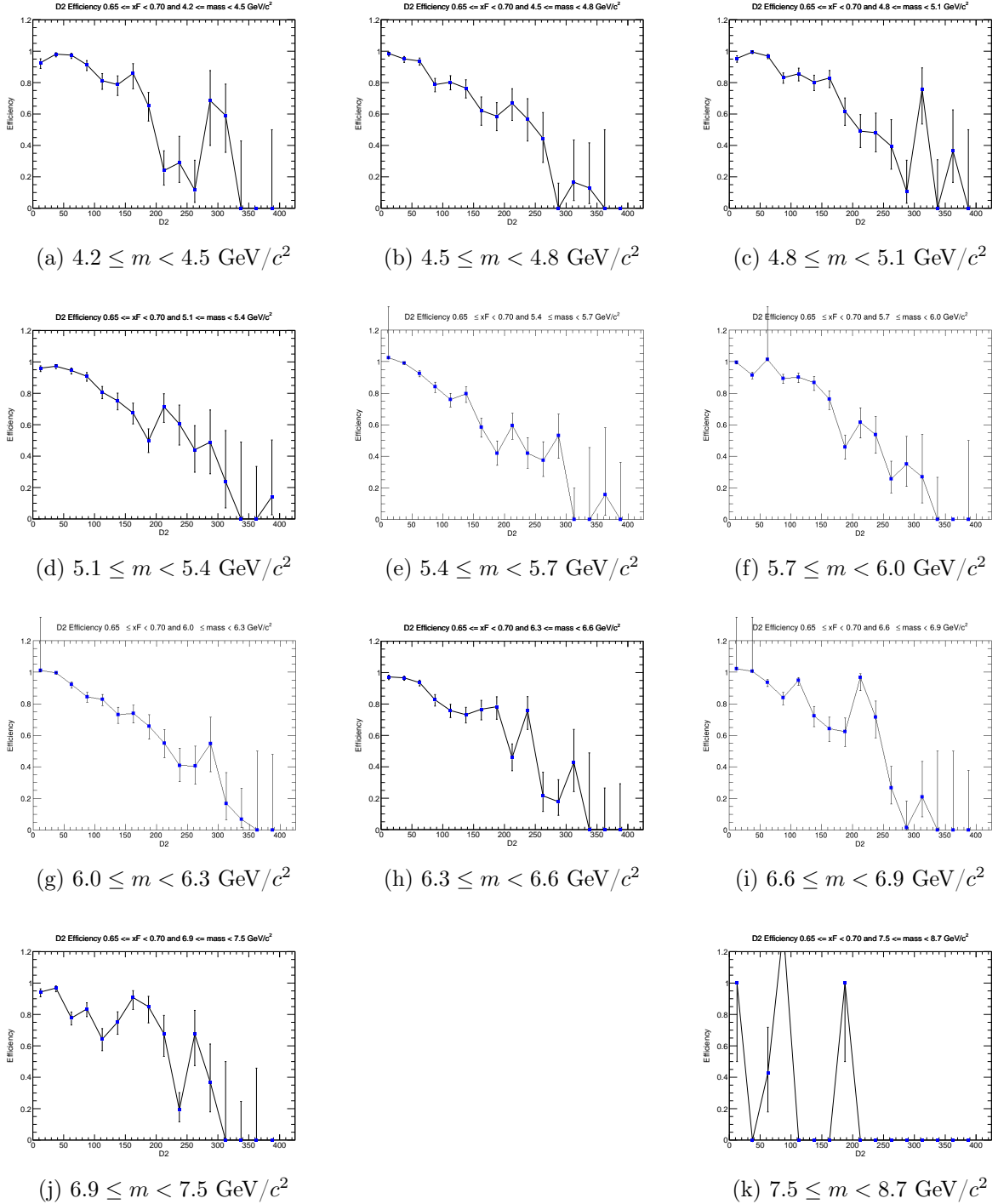


Figure 30: Efficiency plots for the x_F bin $0.65 \leq x_F < 0.70$.

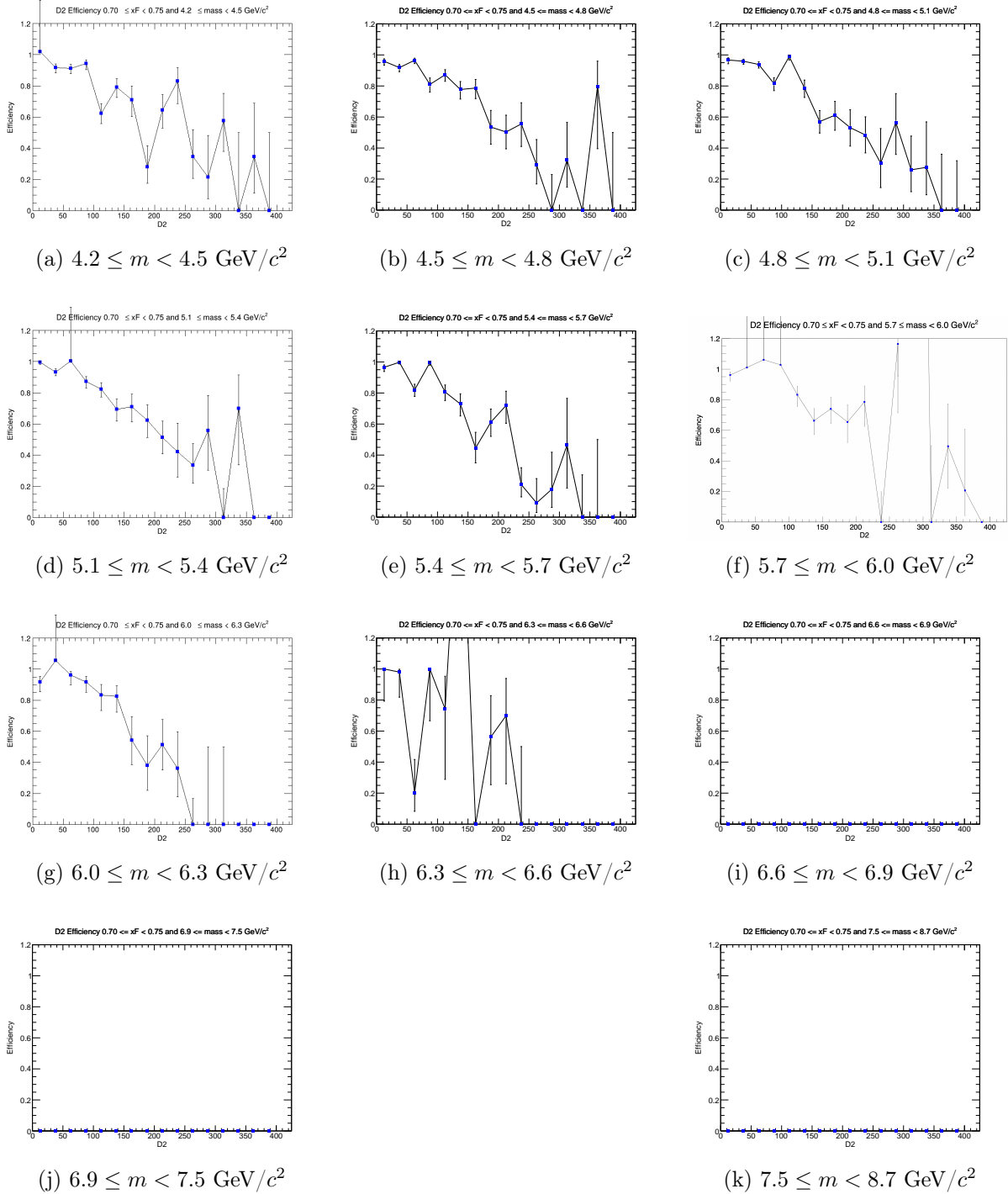


Figure 31: Efficiency plots for the x_F bin $0.70 \leq x_F < 0.75$.

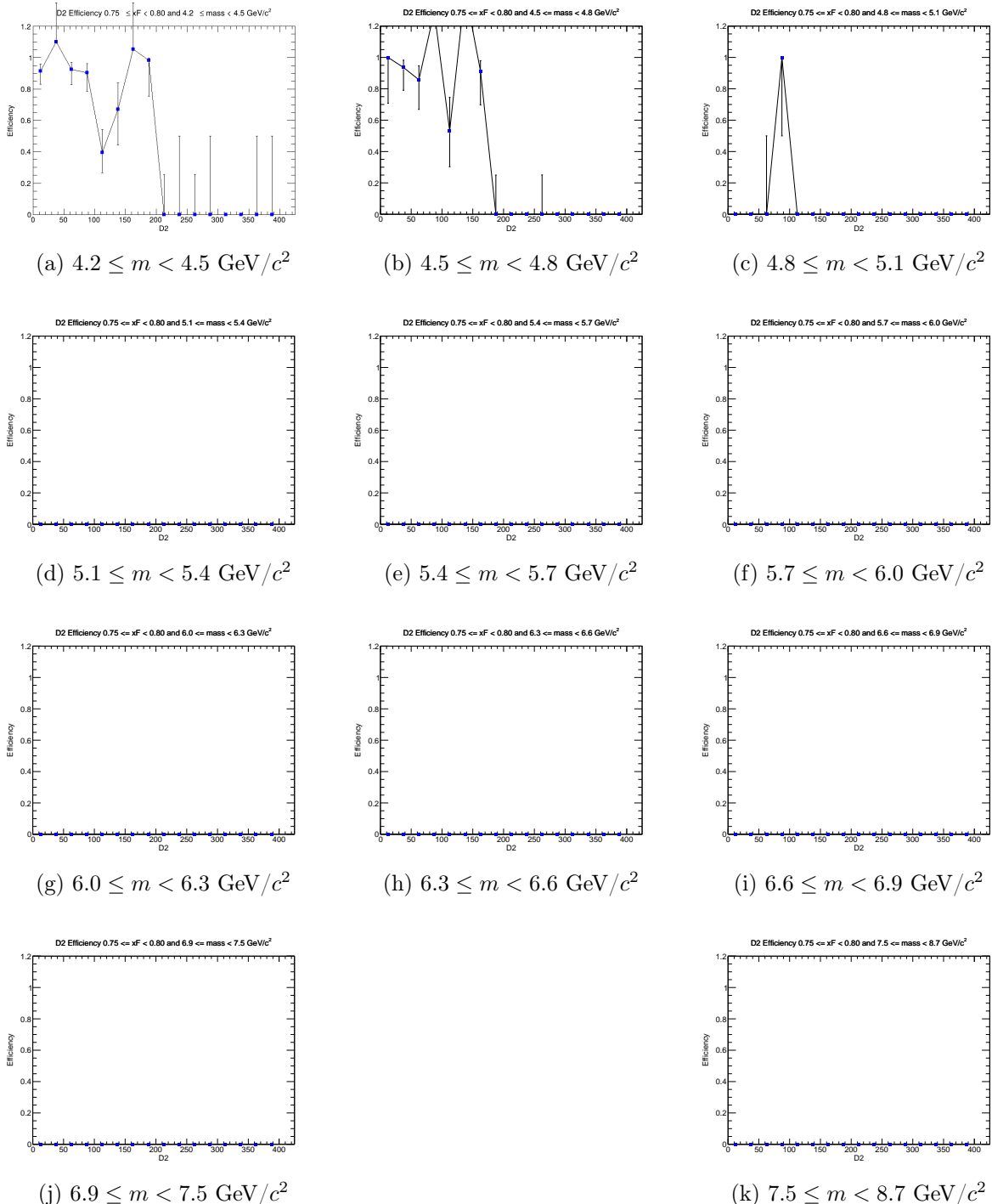


Figure 32: Efficiency plots for the x_F bin $0.75 \leq x_F < 0.80$.

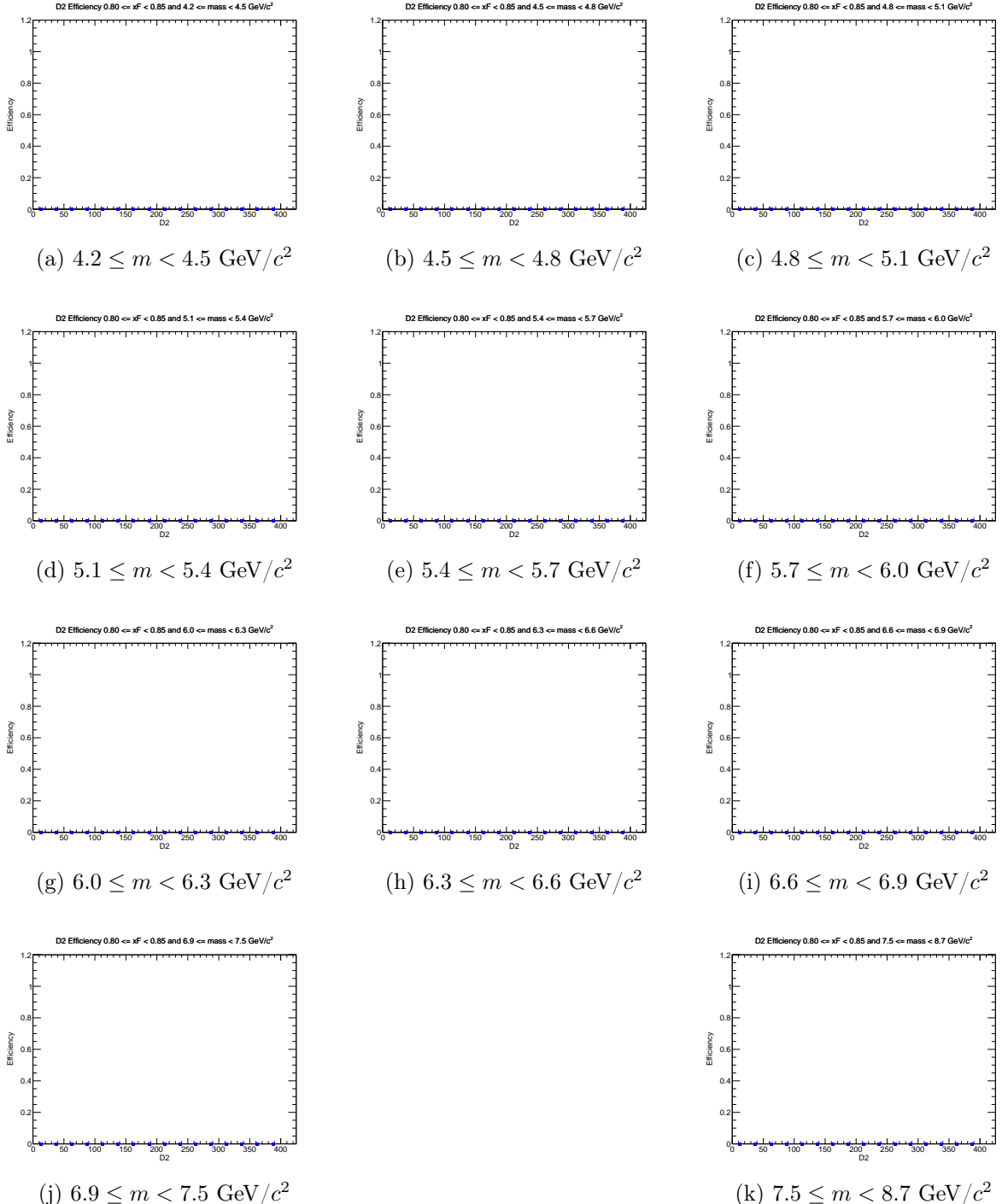


Figure 33: Efficiency plots for the x_F bin $0.80 \leq x_F < 0.85$.

Several bins exhibit unphysical average efficiencies, with some values equal to zero and others exceeding 100%. Therefore, only the bins with valid, non-zero kTracker efficiencies are included in the final cross-section calculation.

231

Table ?? summary of the calculated average efficiencies and their uncertainties for each kinematic bin using the RS-67 LH₂ dataset.

Table 1: Average Efficiency and Errors for Bins in x_F and Mass

x_F Bin	Mass Bin (GeV)	N_{events}	$\langle \epsilon \rangle$	$\delta_{\text{stat}} \langle \epsilon \rangle$	$\delta_{\text{prop}} \langle \epsilon \rangle$	$1/\langle \epsilon \rangle$	$\delta(1/\langle \epsilon \rangle)$
[0.0, 0.05)	[4.5, 4.8)	9	0.1378	0.0878	0.0248	7.258	1.305
[0.0, 0.05)	[4.8, 5.1)	40	0.8807	0.0827	0.0209	1.135	0.027
[0.0, 0.05)	[5.1, 5.4)	72	0.6521	0.0167	0.0216	1.534	0.051
[0.0, 0.05)	[5.4, 5.7)	66	0.6728	0.0262	0.0119	1.486	0.026
[0.0, 0.05)	[5.7, 6.0)	37	0.5828	0.0505	0.0174	1.716	0.051
[0.0, 0.05)	[6.0, 6.3)	26	0.6369	0.0445	0.0190	1.570	0.047
[0.0, 0.05)	[6.3, 6.6)	15	0.5970	0.0532	0.0313	1.675	0.088
[0.0, 0.05)	[6.6, 6.9)	12	0.7055	0.0394	0.0250	1.417	0.050
[0.0, 0.05)	[6.9, 7.5)	9	0.6253	0.0865	0.0272	1.599	0.070
[0.0, 0.05)	[7.5, 8.7)	1	0.6066	0.0000	0.0595	1.649	0.162
[0.05, 0.1)	[4.5, 4.8)	39	0.2746	0.0516	0.0222	3.642	0.294
[0.05, 0.1)	[4.8, 5.1)	81	0.5004	0.0360	0.0185	1.999	0.074
[0.05, 0.1)	[5.1, 5.4)	95	0.7206	0.0381	0.0099	1.388	0.019
[0.05, 0.1)	[5.4, 5.7)	77	0.6718	0.0192	0.0122	1.488	0.027
[0.05, 0.1)	[5.7, 6.0)	53	0.7379	0.0231	0.0122	1.355	0.022
[0.05, 0.1)	[6.0, 6.3)	39	0.7318	0.0325	0.0117	1.367	0.022
[0.05, 0.1)	[6.3, 6.6)	25	0.5964	0.0379	0.0204	1.677	0.057
[0.05, 0.1)	[6.6, 6.9)	5	0.5670	0.1215	0.0382	1.764	0.119
[0.05, 0.1)	[6.9, 7.5)	7	0.6487	0.0764	0.0268	1.541	0.064
[0.05, 0.1)	[7.5, 8.7)	6	0.5979	0.1095	0.0270	1.672	0.075
[0.1, 0.15)	[4.5, 4.8)	96	0.5701	0.0284	0.0173	1.754	0.053
[0.1, 0.15)	[4.8, 5.1)	137	0.6224	0.0151	0.0144	1.607	0.037
[0.1, 0.15)	[5.1, 5.4)	132	0.5965	0.0152	0.0114	1.676	0.032
[0.1, 0.15)	[5.4, 5.7)	87	0.6659	0.0247	0.0091	1.502	0.021
[0.1, 0.15)	[5.7, 6.0)	76	0.6958	0.0183	0.0088	1.437	0.018
[0.1, 0.15)	[6.0, 6.3)	52	0.7145	0.0263	0.0102	1.400	0.020
[0.1, 0.15)	[6.3, 6.6)	28	0.7879	0.0218	0.0113	1.269	0.018
[0.1, 0.15)	[6.6, 6.9)	10	0.7518	0.0446	0.0193	1.330	0.034
[0.1, 0.15)	[6.9, 7.5)	11	0.6798	0.0405	0.0167	1.471	0.036
[0.1, 0.15)	[7.5, 8.7)	7	0.7011	0.0352	0.0140	1.426	0.029
[0.15, 0.2)	[4.5, 4.8)	167	0.6997	0.0217	0.0132	1.429	0.027
[0.15, 0.2)	[4.8, 5.1)	231	0.5373	0.0098	0.0088	1.861	0.030
[0.15, 0.2)	[5.1, 5.4)	201	0.6974	0.0126	0.0070	1.434	0.014
[0.15, 0.2)	[5.4, 5.7)	113	0.6925	0.0214	0.0087	1.444	0.018
[0.15, 0.2)	[5.7, 6.0)	94	0.7358	0.0197	0.0088	1.359	0.016
[0.15, 0.2)	[6.0, 6.3)	67	0.7156	0.0175	0.0089	1.397	0.017
[0.15, 0.2)	[6.3, 6.6)	35	0.7728	0.0346	0.0100	1.294	0.017
[0.15, 0.2)	[6.6, 6.9)	16	0.6784	0.0492	0.0176	1.474	0.038
[0.15, 0.2)	[6.9, 7.5)	12	0.6677	0.0281	0.0149	1.498	0.033
[0.15, 0.2)	[7.5, 8.7)	3	0.6570	0.1554	0.0400	1.522	0.093
[0.2, 0.25)	[4.2, 4.5)	181	0.5438	0.0217	0.0128	1.839	0.043

Continued on next page

Table 1: (Continued)

x_F Bin	Mass Bin (GeV)	N_{events}	$\langle \epsilon \rangle$	$\delta_{\text{stat}} \langle \epsilon \rangle$	$\delta_{\text{prop}} \langle \epsilon \rangle$	$1/\langle \epsilon \rangle$	$\delta(1/\langle \epsilon \rangle)$
[0.2, 0.25)	[4.5, 4.8)	281	0.6018	0.0152	0.0074	1.662	0.021
[0.2, 0.25)	[4.8, 5.1)	269	0.7047	0.0114	0.0057	1.419	0.012
[0.2, 0.25)	[5.1, 5.4)	206	0.6898	0.0124	0.0057	1.450	0.012
[0.2, 0.25)	[5.4, 5.7)	143	0.6979	0.0163	0.0067	1.433	0.014
[0.2, 0.25)	[5.7, 6.0)	106	0.7908	0.0127	0.0062	1.265	0.010
[0.2, 0.25)	[6.0, 6.3)	54	0.7371	0.0250	0.0086	1.357	0.016
[0.2, 0.25)	[6.3, 6.6)	46	0.7367	0.0252	0.0097	1.357	0.018
[0.2, 0.25)	[6.6, 6.9)	21	0.7909	0.0341	0.0111	1.264	0.018
[0.2, 0.25)	[6.9, 7.5)	10	0.6953	0.0456	0.0153	1.438	0.032
[0.2, 0.25)	[7.5, 8.7)	6	0.7790	0.0427	0.0117	1.284	0.019
[0.25, 0.3)	[4.2, 4.5)	363	0.7031	0.0120	0.0075	1.422	0.015
[0.25, 0.3)	[4.5, 4.8)	402	0.7172	0.0073	0.0053	1.394	0.010
[0.25, 0.3)	[4.8, 5.1)	316	0.7115	0.0135	0.0046	1.406	0.009
[0.25, 0.3)	[5.1, 5.4)	243	0.7125	0.0110	0.0052	1.404	0.010
[0.25, 0.3)	[5.4, 5.7)	179	0.7724	0.0123	0.0055	1.295	0.009
[0.25, 0.3)	[5.7, 6.0)	89	0.7356	0.0196	0.0074	1.359	0.014
[0.25, 0.3)	[6.0, 6.3)	60	0.7620	0.0156	0.0078	1.312	0.013
[0.25, 0.3)	[6.3, 6.6)	38	0.7720	0.0232	0.0083	1.295	0.014
[0.25, 0.3)	[6.6, 6.9)	26	0.6924	0.0382	0.0134	1.444	0.028
[0.25, 0.3)	[6.9, 7.5)	24	0.7399	0.0379	0.0104	1.352	0.019
[0.25, 0.3)	[7.5, 8.7)	2	0.5631	0.0363	0.0336	1.776	0.106
[0.3, 0.35)	[4.2, 4.5)	542	0.7566	0.0065	0.0051	1.322	0.009
[0.3, 0.35)	[4.5, 4.8)	488	0.7802	0.0082	0.0037	1.282	0.006
[0.3, 0.35)	[4.8, 5.1)	381	0.7314	0.0087	0.0039	1.367	0.007
[0.3, 0.35)	[5.1, 5.4)	271	0.7999	0.0086	0.0038	1.250	0.006
[0.3, 0.35)	[5.4, 5.7)	185	0.7186	0.0118	0.0047	1.392	0.009
[0.3, 0.35)	[5.7, 6.0)	93	0.7165	0.0225	0.0063	1.396	0.012
[0.3, 0.35)	[6.0, 6.3)	60	0.7233	0.0225	0.0083	1.383	0.016
[0.3, 0.35)	[6.3, 6.6)	45	0.7940	0.0231	0.0074	1.259	0.012
[0.3, 0.35)	[6.6, 6.9)	25	0.7720	0.0154	0.0113	1.295	0.019
[0.3, 0.35)	[6.9, 7.5)	19	0.7341	0.0488	0.0124	1.362	0.023
[0.3, 0.35)	[7.5, 8.7)	9	0.7511	0.0670	0.0119	1.331	0.021
[0.35, 0.4)	[4.2, 4.5)	625	0.8121	0.0077	0.0034	1.231	0.005
[0.35, 0.4)	[4.5, 4.8)	543	0.7329	0.0080	0.0034	1.364	0.006
[0.35, 0.4)	[4.8, 5.1)	402	0.7561	0.0070	0.0036	1.323	0.006
[0.35, 0.4)	[5.1, 5.4)	281	0.7953	0.0085	0.0038	1.257	0.006
[0.35, 0.4)	[5.4, 5.7)	147	0.7652	0.0140	0.0046	1.307	0.008
[0.35, 0.4)	[5.7, 6.0)	110	0.7670	0.0171	0.0054	1.304	0.009
[0.35, 0.4)	[6.0, 6.3)	68	0.8024	0.0186	0.0064	1.246	0.010
[0.35, 0.4)	[6.3, 6.6)	43	0.7917	0.0221	0.0077	1.263	0.012
[0.35, 0.4)	[6.6, 6.9)	20	0.7471	0.0310	0.0124	1.339	0.022
[0.35, 0.4)	[6.9, 7.5)	19	0.7659	0.0476	0.0091	1.306	0.016
[0.35, 0.4)	[7.5, 8.7)	8	0.6464	0.0596	0.0164	1.547	0.039
[0.4, 0.45)	[4.2, 4.5)	652	0.7735	0.0068	0.0034	1.293	0.006
[0.4, 0.45)	[4.5, 4.8)	497	0.7426	0.0113	0.0031	1.347	0.006
[0.4, 0.45)	[4.8, 5.1)	400	0.7471	0.0075	0.0032	1.339	0.006
[0.4, 0.45)	[5.1, 5.4)	244	0.7470	0.0091	0.0041	1.339	0.007
[0.4, 0.45)	[5.4, 5.7)	178	0.7796	0.0111	0.0040	1.283	0.007

Continued on next page

Table 1: (Continued)

x_F Bin	Mass Bin (GeV)	N_{events}	$\langle \epsilon \rangle$	$\delta_{\text{stat}} \langle \epsilon \rangle$	$\delta_{\text{prop}} \langle \epsilon \rangle$	$1/\langle \epsilon \rangle$	$\delta(1/\langle \epsilon \rangle)$
[0.4, 0.45)	[5.7, 6.0)	94	0.7949	0.0181	0.0054	1.258	0.008
[0.4, 0.45)	[6.0, 6.3)	82	0.8039	0.0141	0.0058	1.244	0.009
[0.4, 0.45)	[6.3, 6.6)	47	0.7396	0.0240	0.0085	1.352	0.016
[0.4, 0.45)	[6.6, 6.9)	24	0.8323	0.0225	0.0085	1.202	0.012
[0.4, 0.45)	[6.9, 7.5)	20	0.7353	0.0435	0.0102	1.360	0.019
[0.4, 0.45)	[7.5, 8.7)	8	0.8233	0.0525	0.0100	1.215	0.015
[0.45, 0.5)	[4.2, 4.5)	671	0.7745	0.0068	0.0030	1.291	0.005
[0.45, 0.5)	[4.5, 4.8)	512	0.7618	0.0060	0.0028	1.313	0.005
[0.45, 0.5)	[4.8, 5.1)	352	0.7306	0.0078	0.0034	1.369	0.006
[0.45, 0.5)	[5.1, 5.4)	219	0.7627	0.0126	0.0043	1.311	0.007
[0.45, 0.5)	[5.4, 5.7)	143	0.8074	0.0098	0.0047	1.239	0.007
[0.45, 0.5)	[5.7, 6.0)	96	0.7845	0.0163	0.0055	1.275	0.009
[0.45, 0.5)	[6.0, 6.3)	58	0.7846	0.0272	0.0073	1.275	0.012
[0.45, 0.5)	[6.3, 6.6)	49	0.7242	0.0193	0.0081	1.381	0.016
[0.45, 0.5)	[6.6, 6.9)	17	0.7580	0.0364	0.0148	1.319	0.026
[0.45, 0.5)	[6.9, 7.5)	27	0.7951	0.0238	0.0064	1.258	0.010
[0.45, 0.5)	[7.5, 8.7)	7	0.8274	0.0525	0.0121	1.209	0.018
[0.5, 0.55)	[4.2, 4.5)	616	0.6899	0.0076	0.0035	1.449	0.007
[0.5, 0.55)	[4.5, 4.8)	395	0.7404	0.0071	0.0034	1.351	0.006
[0.5, 0.55)	[4.8, 5.1)	285	0.7299	0.0106	0.0037	1.370	0.007
[0.5, 0.55)	[5.1, 5.4)	207	0.7855	0.0108	0.0038	1.273	0.006
[0.5, 0.55)	[5.4, 5.7)	152	0.7783	0.0082	0.0042	1.285	0.007
[0.5, 0.55)	[5.7, 6.0)	78	0.7854	0.0165	0.0062	1.273	0.010
[0.5, 0.55)	[6.0, 6.3)	42	0.7132	0.0300	0.0093	1.402	0.018
[0.5, 0.55)	[6.3, 6.6)	38	0.8216	0.0208	0.0073	1.217	0.011
[0.5, 0.55)	[6.6, 6.9)	16	0.7818	0.0286	0.0137	1.279	0.022
[0.5, 0.55)	[6.9, 7.5)	14	0.8153	0.0477	0.0107	1.227	0.016
[0.5, 0.55)	[7.5, 8.7)	10	0.7404	0.0443	0.0111	1.351	0.020
[0.55, 0.6)	[4.2, 4.5)	486	0.7795	0.0079	0.0032	1.283	0.005
[0.55, 0.6)	[4.5, 4.8)	385	0.7572	0.0073	0.0033	1.321	0.006
[0.55, 0.6)	[4.8, 5.1)	245	0.7574	0.0105	0.0041	1.320	0.007
[0.55, 0.6)	[5.1, 5.4)	153	0.7870	0.0131	0.0045	1.271	0.007
[0.55, 0.6)	[5.4, 5.7)	90	0.8021	0.0166	0.0058	1.247	0.009
[0.55, 0.6)	[5.7, 6.0)	59	0.7335	0.0184	0.0064	1.363	0.012
[0.55, 0.6)	[6.0, 6.3)	42	0.8234	0.0219	0.0070	1.214	0.010
[0.55, 0.6)	[6.3, 6.6)	22	0.7949	0.0223	0.0096	1.258	0.015
[0.55, 0.6)	[6.6, 6.9)	16	0.8082	0.0364	0.0122	1.237	0.019
[0.55, 0.6)	[6.9, 7.5)	14	0.7432	0.0579	0.0109	1.346	0.020
[0.55, 0.6)	[7.5, 8.7)	5	0.7910	0.0674	0.0155	1.264	0.025
[0.6, 0.65)	[4.2, 4.5)	380	0.7973	0.0086	0.0034	1.254	0.005
[0.6, 0.65)	[4.5, 4.8)	251	0.7772	0.0104	0.0042	1.287	0.007
[0.6, 0.65)	[4.8, 5.1)	164	0.7728	0.0112	0.0046	1.294	0.008
[0.6, 0.65)	[5.1, 5.4)	108	0.8356	0.0156	0.0044	1.197	0.006
[0.6, 0.65)	[5.4, 5.7)	66	0.8310	0.0158	0.0060	1.203	0.009
[0.6, 0.65)	[5.7, 6.0)	51	0.7211	0.0237	0.0078	1.387	0.015
[0.6, 0.65)	[6.0, 6.3)	38	0.8297	0.0284	0.0081	1.205	0.012
[0.6, 0.65)	[6.3, 6.6)	19	0.7875	0.0322	0.0096	1.270	0.015
[0.6, 0.65)	[6.6, 6.9)	12	0.9017	0.0334	0.0086	1.109	0.011

Continued on next page

Table 1: (Continued)

x_F Bin	Mass Bin (GeV)	N_{events}	$\langle \epsilon \rangle$	$\delta_{\text{stat}} \langle \epsilon \rangle$	$\delta_{\text{prop}} \langle \epsilon \rangle$	$1/\langle \epsilon \rangle$	$\delta(1/\langle \epsilon \rangle)$
[0.6, 0.65)	[6.9, 7.5)	10	0.8154	0.0785	0.0137	1.226	0.021
[0.6, 0.65)	[7.5, 8.7)	3	0.8549	0.1118	0.0236	1.170	0.032
[0.65, 0.7)	[4.2, 4.5)	248	0.7996	0.0124	0.0041	1.251	0.006
[0.65, 0.7)	[4.5, 4.8)	181	0.7809	0.0098	0.0046	1.281	0.008
[0.65, 0.7)	[4.8, 5.1)	111	0.8258	0.0126	0.0049	1.211	0.007
[0.65, 0.7)	[5.1, 5.4)	91	0.8077	0.0142	0.0053	1.238	0.008
[0.65, 0.7)	[5.4, 5.7)	55	0.7491	0.0220	0.0068	1.335	0.012
[0.65, 0.7)	[5.7, 6.0)	31	0.8202	0.0300	0.0094	1.219	0.014
[0.65, 0.7)	[6.0, 6.3)	23	0.7967	0.0288	0.0103	1.255	0.016
[0.65, 0.7)	[6.3, 6.6)	9	0.7798	0.0436	0.0173	1.282	0.028
[0.65, 0.7)	[6.6, 6.9)	9	0.8424	0.0382	0.0151	1.187	0.021
[0.65, 0.7)	[6.9, 7.5)	15	0.7883	0.0219	0.0162	1.269	0.026
[0.65, 0.7)	[7.5, 8.7)	5	0.0786	0.0548	0.0410	12.717	6.635
[0.7, 0.75)	[4.2, 4.5)	167	0.7450	0.0129	0.0057	1.342	0.010
[0.7, 0.75)	[4.5, 4.8)	136	0.7774	0.0134	0.0055	1.286	0.009
[0.7, 0.75)	[4.8, 5.1)	86	0.7999	0.0178	0.0068	1.250	0.011
[0.7, 0.75)	[5.1, 5.4)	44	0.7882	0.0227	0.0106	1.269	0.017
[0.7, 0.75)	[5.4, 5.7)	25	0.7779	0.0380	0.0115	1.286	0.019
[0.7, 0.75)	[5.7, 6.0)	17	0.8597	0.0364	0.0185	1.163	0.025
[0.7, 0.75)	[6.0, 6.3)	15	0.7732	0.0519	0.0268	1.293	0.045
[0.7, 0.75)	[6.3, 6.6)	11	0.8705	0.1232	0.0475	1.149	0.063
[0.75, 0.8)	[4.2, 4.5)	114	0.7278	0.0267	0.0099	1.374	0.019
[0.75, 0.8)	[4.5, 4.8)	51	0.9280	0.0492	0.0090	1.078	0.010
[0.75, 0.8)	[4.8, 5.1)	34	0.0947	0.0366	0.0160	10.559	1.783

3.3 Trigger Efficiency

In DocDB 10795 Kenichi performed a trigger efficiency study in support of Hugo's charmonium analysis. This study showed an efficiency of 0.87 ± 0.10 independent of kinematic bin. This study will need to be redone for the DY region $4.2 < M < 8.0$. For this purposes of this release, however, we have slightly enlarged the range of the error to include the possibility of a lower efficiency. We have adopted the value $\epsilon_{\text{trigger}} = 0.845 \pm 0.125$ temporarily. We note that this will be the largest contributor to the systematic error described in the next section.

4 Systematic Uncertainties

A comprehensive evaluation of systematic uncertainties is essential for a precision cross-section measurement. The main sources of systematic uncertainty in this analysis include:

- **Luminosity Determination:** Uncertainty in the incident proton flux, target density, and length.
- **Acceptance Correction:** Uncertainty stemming from the MC statistics and the physics model used to generate the Drell-Yan events (e.g., the input PDFs).
- **Reconstruction Efficiency:** Uncertainty from the statistics of the clean and messy MC samples, and the method used to average over the data's occupancy distribution.
- **Background Subtraction:** Uncertainty in the normalization of the empty flask and combinatorial backgrounds.

252 • **Event Selection:** Variation of the analysis cuts to test the stability of the final result.
253 A study of the systematic effect of the combinatoric background subtraction is underway (see
254 DocDB 11307), but this is expected to be purely statistical and not systematic.
255 In this report we have computed a systematic uncertainty from three sources: the recon-
256 struction efficiency, the acceptance, and the trigger efficiency. Those corrections are described
257 in detail in the previous section. In each case we computed the fractional error in the correction
258 and applied that fraction to the corrected yield in Equation 2 to obtain the absolute systematic
259 error. The three systematic errors were added in quadrature. This total systematic error is
260 displayed as an error band in the plots in the next section.

261 5 Results: Double-Differential Cross-Section

262 Following the application of all corrections and background subtraction procedures, the Drell-
263 Yan double-differential cross-section, $M^3 d^2\sigma/(dM dx_F)$, was extracted for the pp collisions at
264 $\sqrt{s} = 15$ GeV. The results are presented in the following figures for all bins of x_F .

265 Each figure displays the measured cross-section as a function of the dimuon invariant mass,
266 M . The error bars on the data points represent the statistical uncertainty, while the error bands
267 show the systematic uncertainties. The data are compared with theoretical predictions based
268 on Next-to-Leading Order (NLO) QCD calculations, using various modern PDF sets.

269 Data points do not appear if the efficiency and/or acceptance for that bin was computed to
270 be zero.

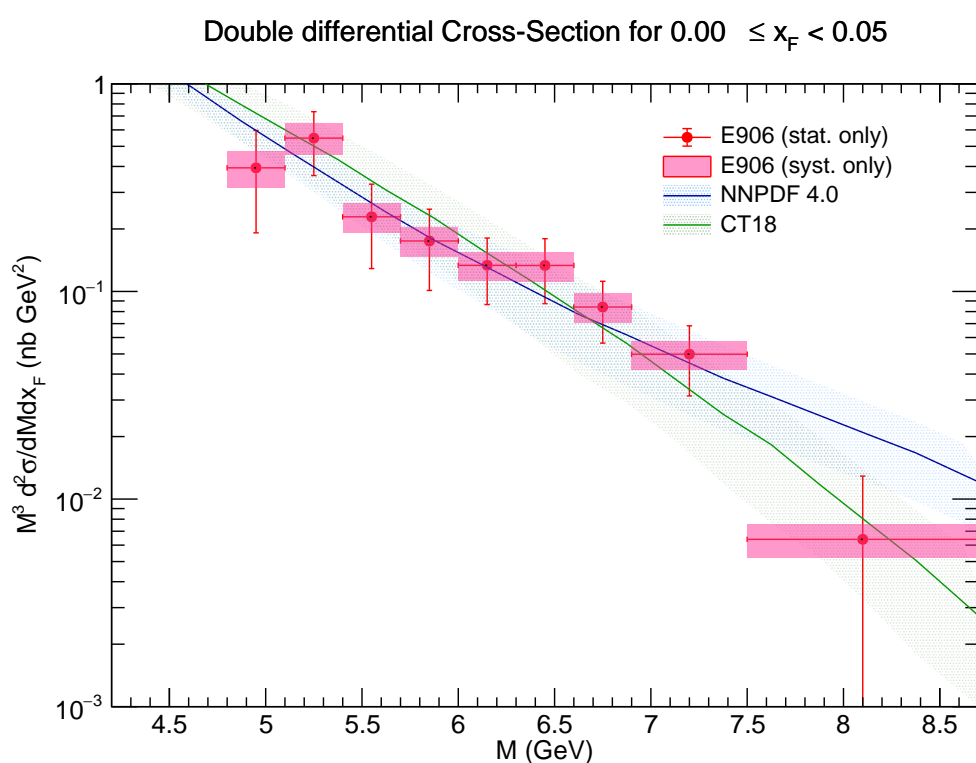


Figure 34: Differential cross-section for x_F bin $0.00 \leq x_F < 0.05$.

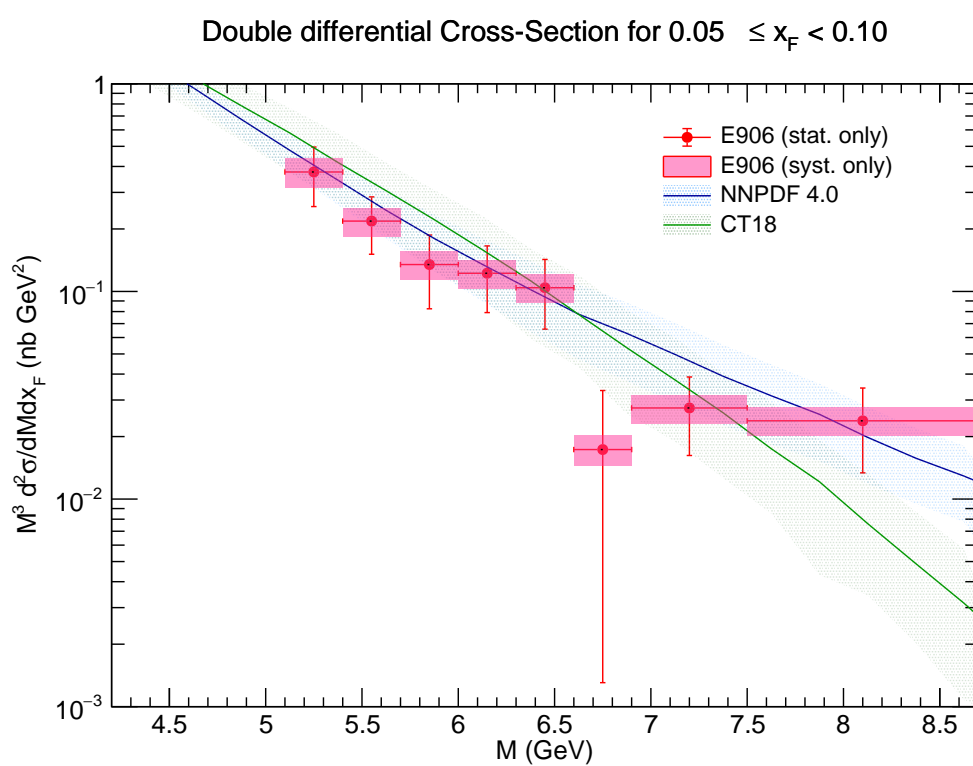


Figure 35: Differential cross-section for x_F bin $0.05 \leq x_F < 0.10$.

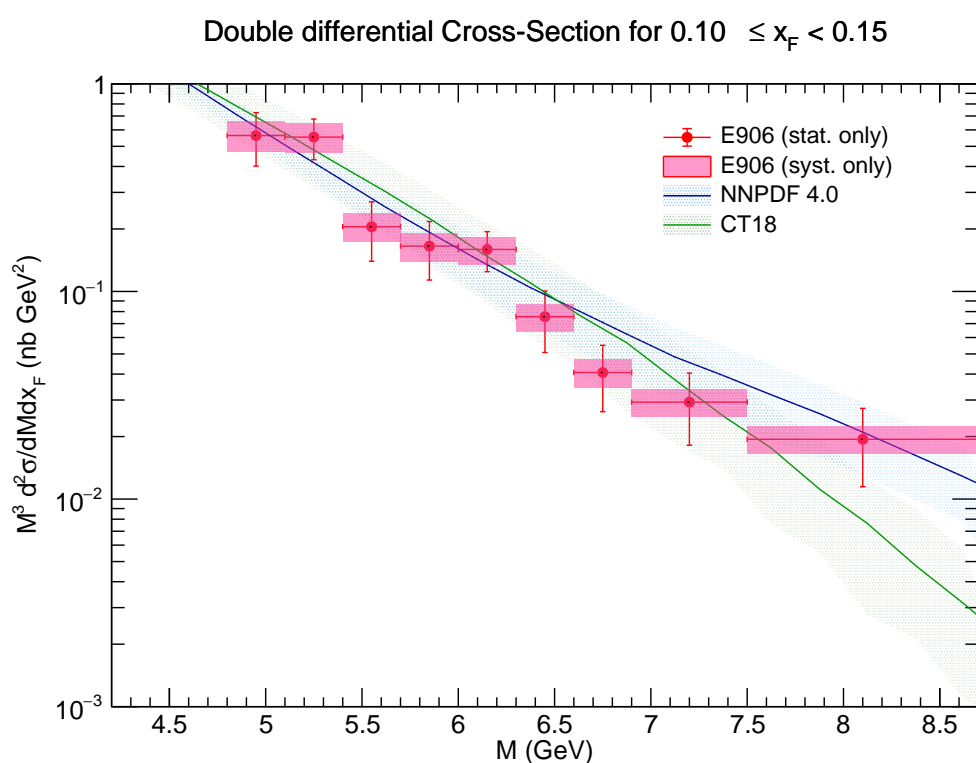


Figure 36: Differential cross-section for x_F bin $0.10 \leq x_F < 0.15$.

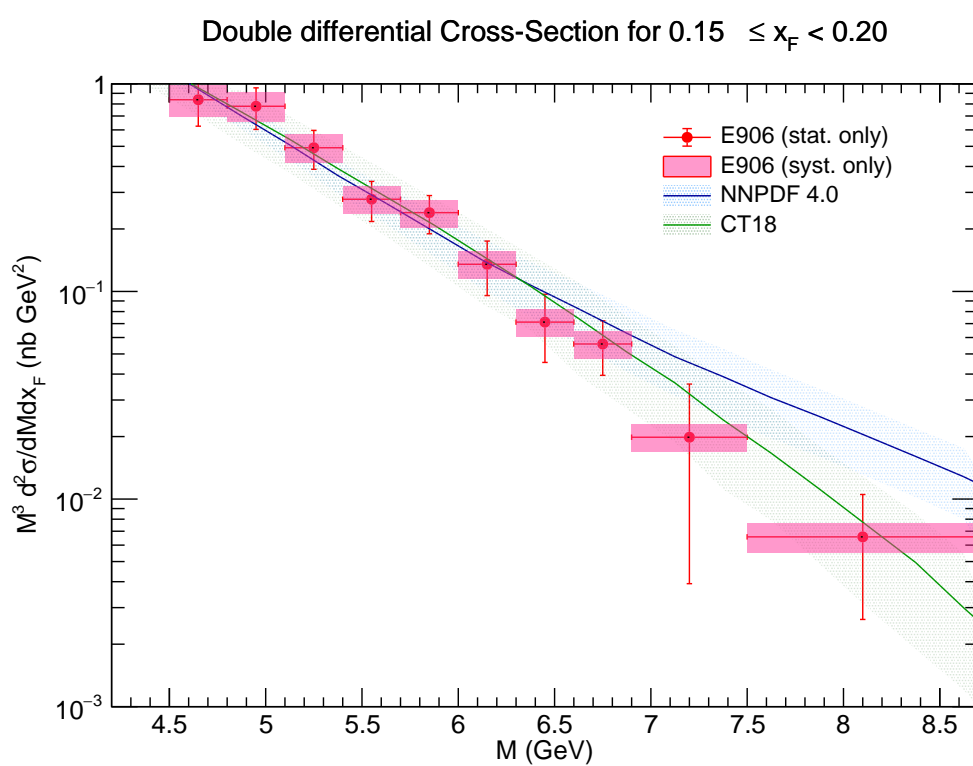


Figure 37: Differential cross-section for x_F bin $0.15 \leq x_F < 0.20$.

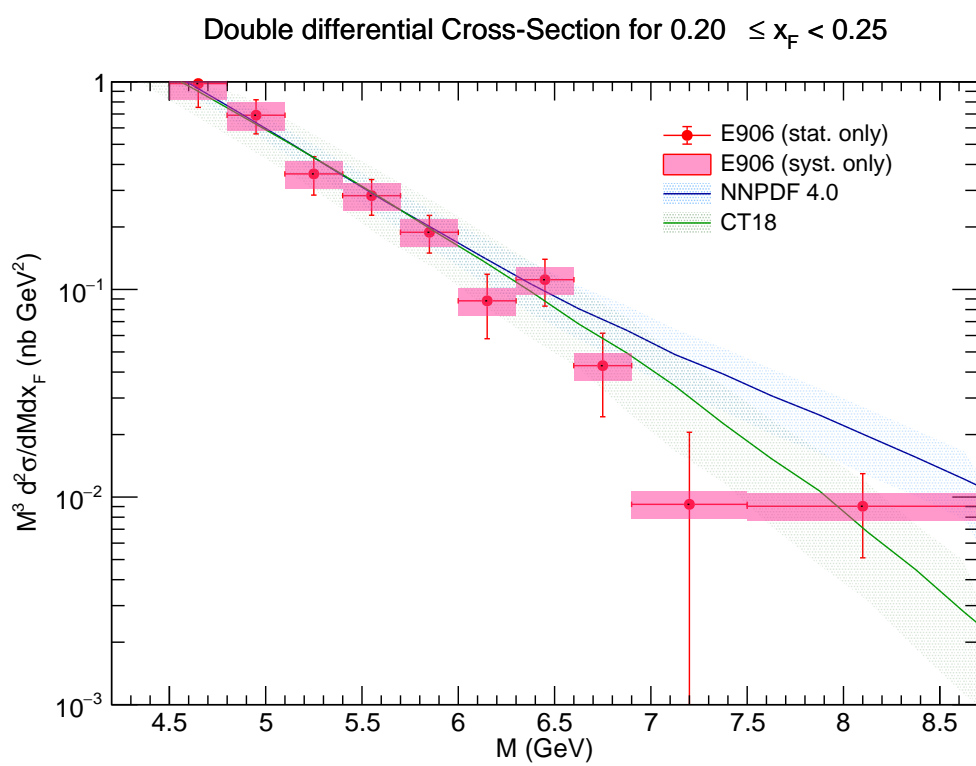


Figure 38: Differential cross-section for x_F bin $0.20 \leq x_F < 0.25$.

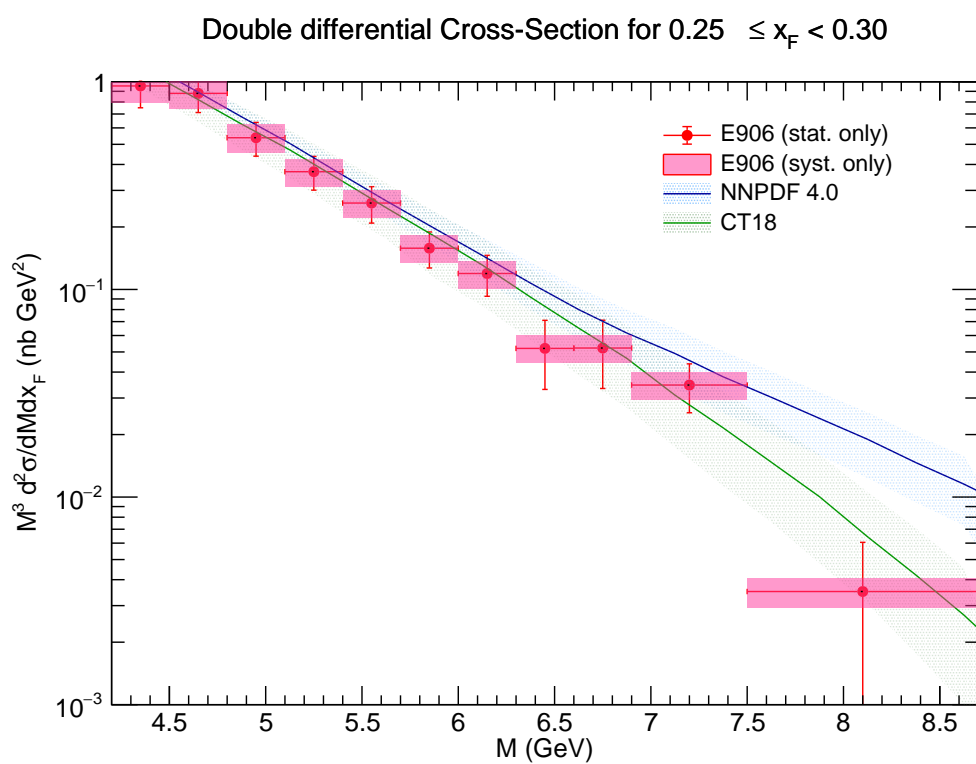


Figure 39: Differential cross-section for x_F bin $0.25 \leq x_F < 0.30$.

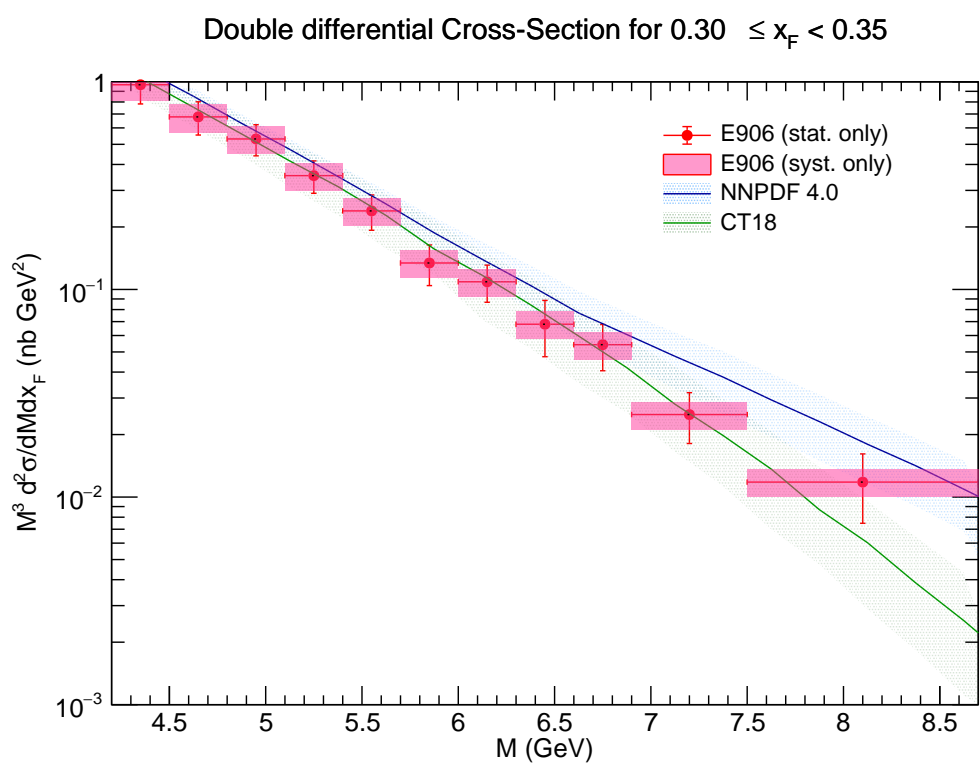


Figure 40: Differential cross-section for x_F bin $0.30 \leq x_F < 0.35$.

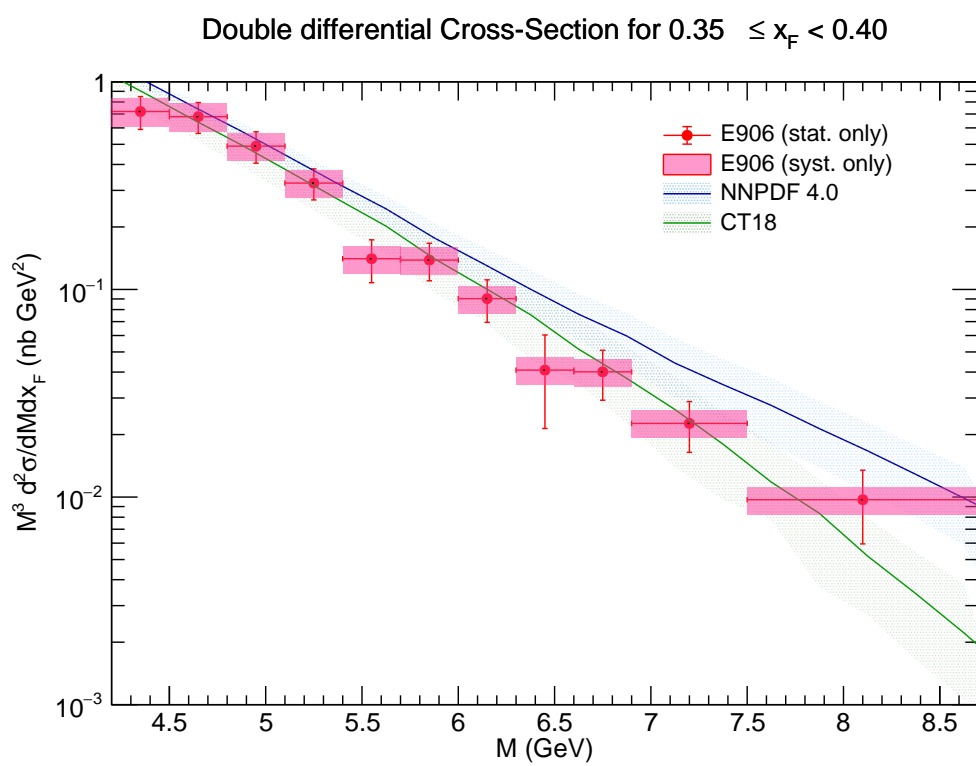


Figure 41: Differential cross-section for x_F bin $0.35 \leq x_F < 0.40$.

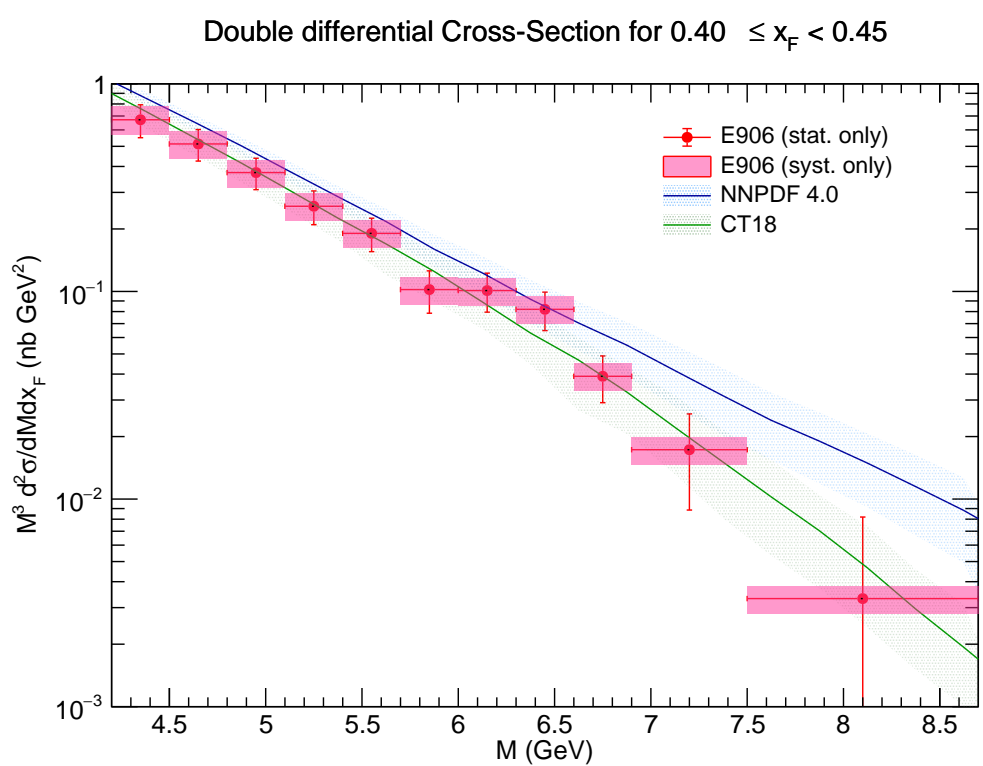


Figure 42: Differential cross-section for x_F bin $0.40 \leq x_F < 0.45$.

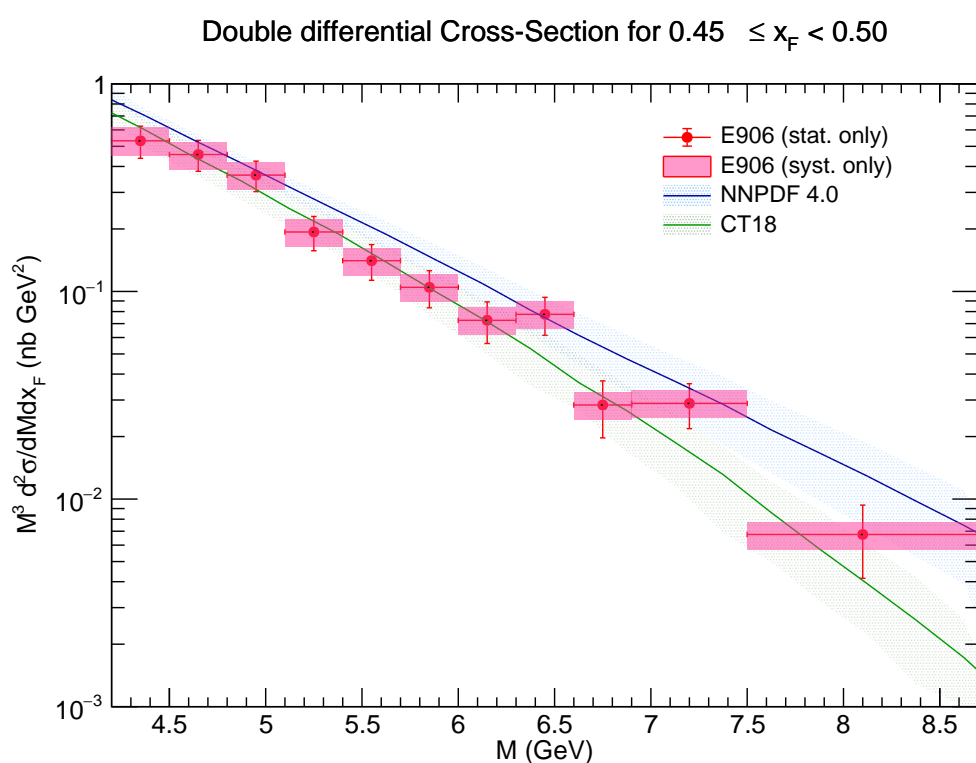


Figure 43: Differential cross-section for x_F bin $0.45 \leq x_F < 0.50$.

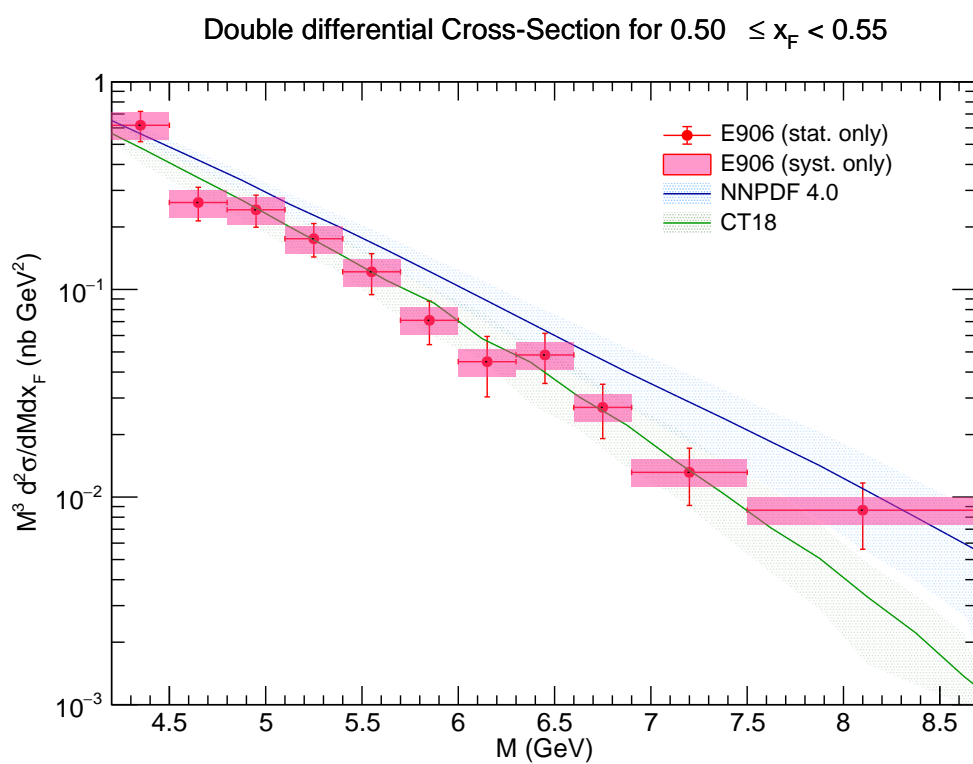


Figure 44: Differential cross-section for x_F bin $0.50 \leq x_F < 0.55$.

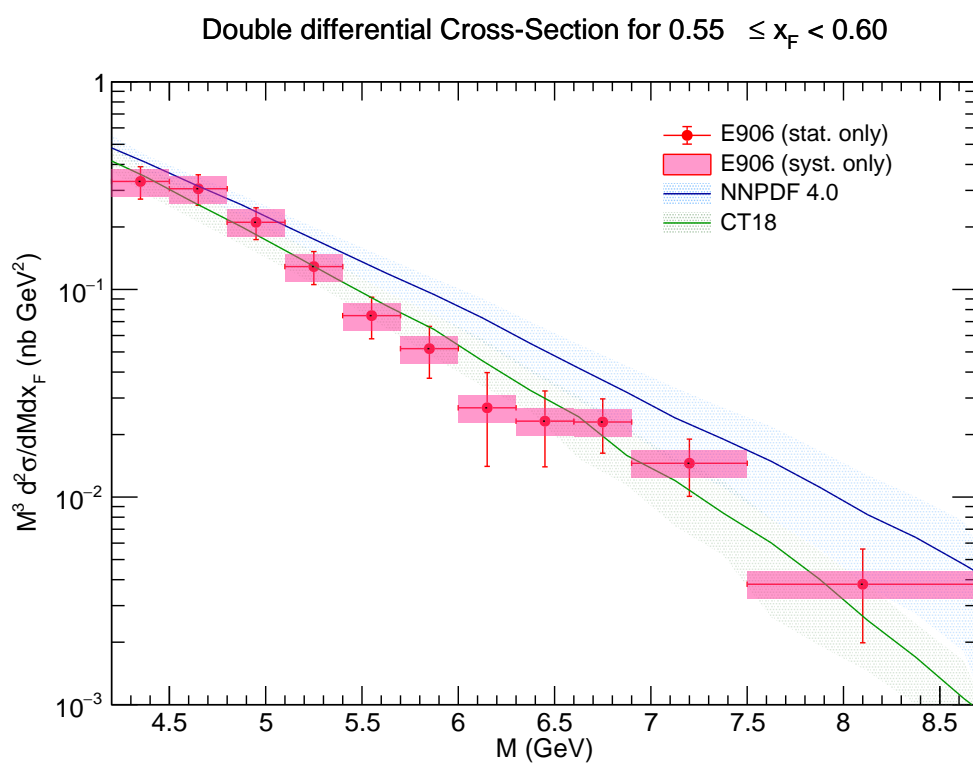


Figure 45: Differential cross-section for x_F bin $0.55 \leq x_F < 0.60$.

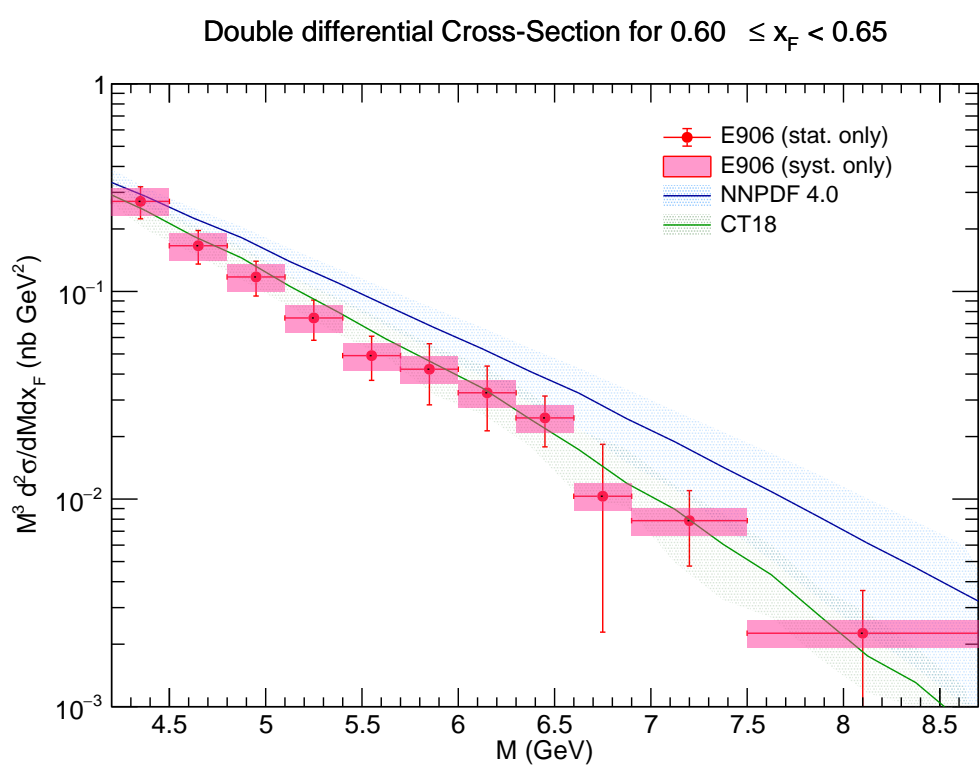


Figure 46: Differential cross-section for x_F bin $0.60 \leq x_F < 0.65$.

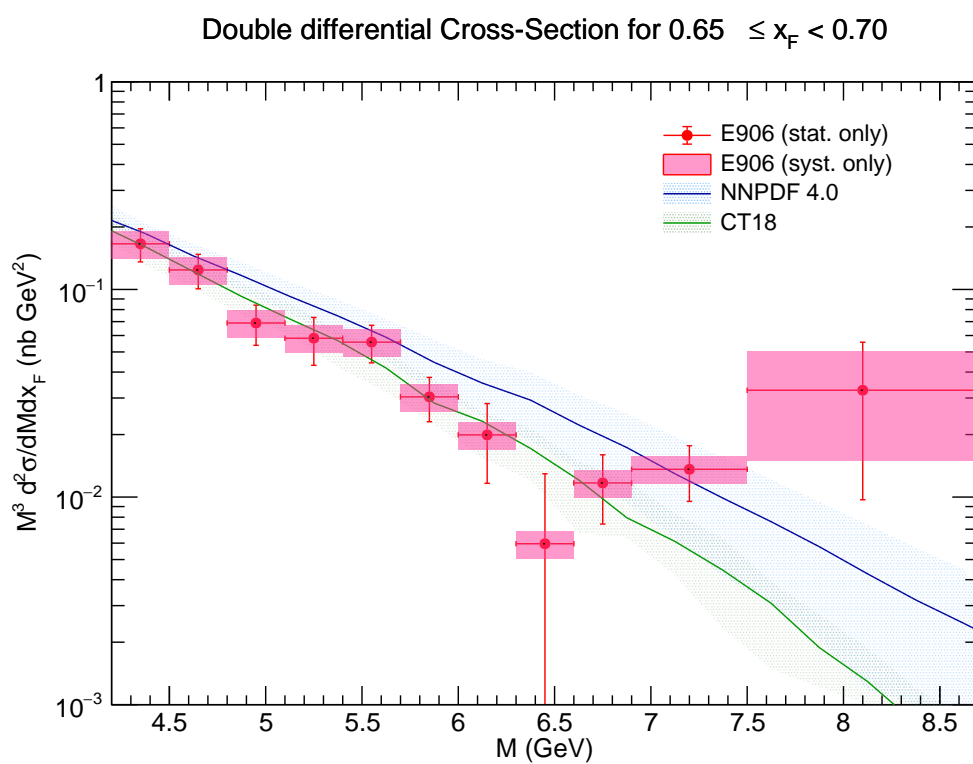


Figure 47: Differential cross-section for x_F bin $0.65 \leq x_F < 0.70$.

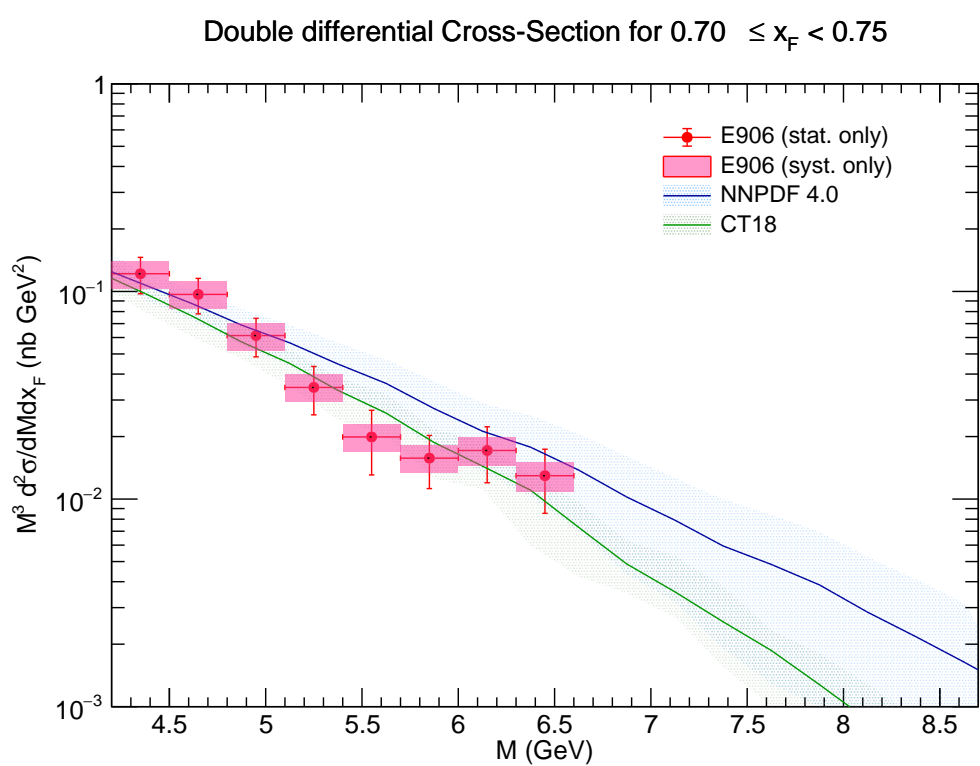


Figure 48: Differential cross-section for x_F bin $0.70 \leq x_F < 0.75$.

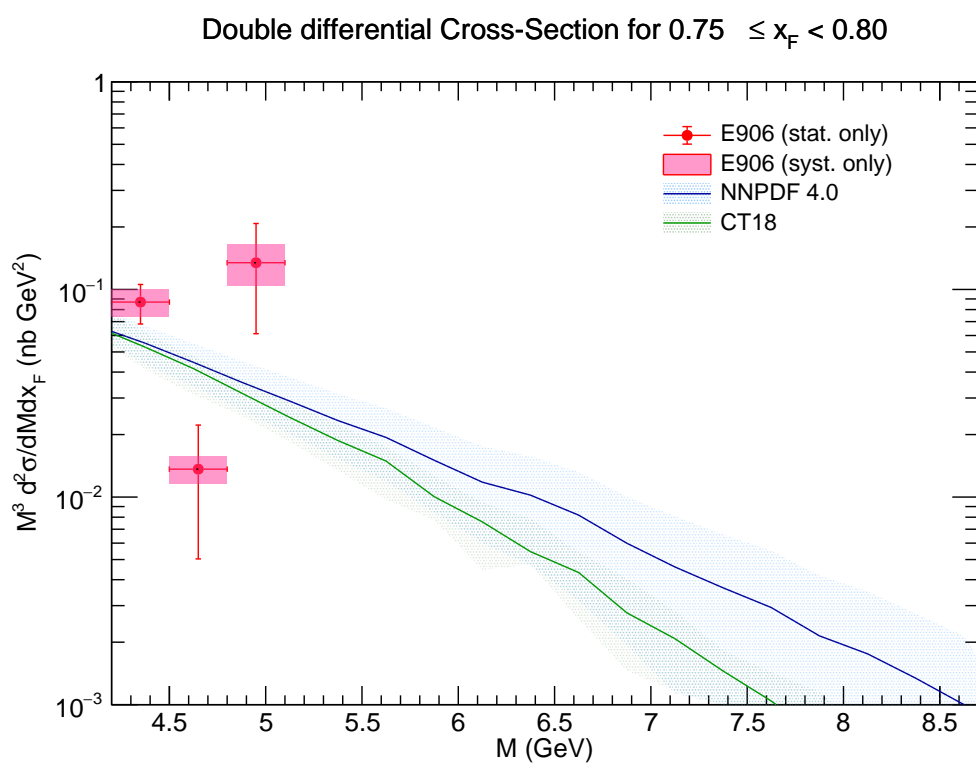


Figure 49: Differential cross-section for x_F bin $0.75 \leq x_F < 0.80$.

271 **6 Discussion and Conclusion**

272 This analysis presents the first measurement of the absolute Drell-Yan cross-section from the
273 Fermilab SeaQuest experiment for pp collisions at 120 GeV. The preliminary results show reasonable
274 agreement with theoretical predictions from NLO QCD using modern PDF sets, although
275 some tension may be apparent in certain kinematic regions. These data, particularly at high
276 x_F , provide valuable new constraints for global PDF fits.

277 The calculation of the reconstruction efficiency correction (Section 3.2) highlights a key challenge of the analysis. In kinematic bins with low statistics, both in the data and the MC samples,
278 the determination of the efficiency can be unreliable. In some cases, statistical fluctuations lead
279 to calculated efficiencies greater than one or zero, and these bins must be excluded from the
280 final result. Future analyses will benefit from MC samples with higher statistics to mitigate this
281 issue.

282 In conclusion, we have developed a comprehensive framework for the measurement of the
283 absolute Drell-Yan cross-section. The results presented here demonstrate the capability of the
284 SeaQuest experiment to probe the antiquark structure of the nucleon in the large- x domain. The
285 final results from this analysis will provide crucial input for resolving long-standing questions
286 about the non-perturbative structure of the proton.

288 **A Appendix: Event Selection Criteria**

289 The analysis relies on a standard set of selection criteria ("cuts") to identify high-quality dimuon
290 events. These are defined for the positive track (μ^+), negative track (μ^-), and the combined
291 dimuon vertex. The cuts are implemented as TCut objects in the ROOT analysis framework.
292 The parameter `beamOffset` accounts for run-dependent shifts in the beam position.

293 **A.1 Positive Track Cuts (chuckCutsPositive_2111v42)**

```
294 chisq1_target < 15 && pz1_st1 > 9 && pz1_st1 < 75 && nHits1 > 13  
295 && x1_t*x1_t + (y1_t-beamOffset)*(y1_t-beamOffset) < 320  
296 && x1_d*x1_d + (y1_d-beamOffset)*(y1_d-beamOffset) < 1100  
297 && x1_d*x1_d + (y1_d-beamOffset)*(y1_d-beamOffset) > 16  
298 && chisq1_target < 1.5*chisq1_upstream && chisq1_target < 1.5*chisq1_dump  
299 && z1_v < -5 && z1_v > -320 && chisq1/(nHits1-5) < 12  
300 && y1_st1/y1_st3 < 1 && abs(abs(px1_st1-px1_st3)-0.416) < 0.008  
301 && abs(py1_st1-py1_st3) < 0.008 && abs(pz1_st1-pz1_st3) < 0.08  
302 && y1_st1*y1_st3 > 0 && abs(py1_st1)>0.02
```

303 **A.2 Negative Track Cuts (chuckCutsNegative_2111v42)**

```
304 chisq2_target < 15 && pz2_st1 > 9 && pz2_st1 < 75 && nHits2 > 13  
305 && x2_t*x2_t + (y2_t-beamOffset)*(y2_t-beamOffset) < 320  
306 && x2_d*x2_d + (y2_d-beamOffset)*(y2_d-beamOffset) < 1100  
307 && x2_d*x2_d + (y2_d-beamOffset)*(y2_d-beamOffset) > 16  
308 && chisq2_target < 1.5*chisq2_upstream && chisq2_target < 1.5*chisq2_dump  
309 && z2_v < -5 && z2_v > -320 && chisq2/(nHits2-5) < 12  
310 && y2_st1/y2_st3 < 1 && abs(abs(px2_st1-px2_st3)-0.416) < 0.008  
311 && abs(py2_st1-py2_st3) < 0.008 && abs(pz2_st1-pz2_st3) < 0.08  
312 && y2_st1*y2_st3 > 0 && abs(py2_st1)>0.02
```

313 **A.3 Dimuon Cuts (chuckCutsDimuon_2111v42)**

```
314 abs(dx) < 0.25 && abs(dy-beamOffset) < 0.22 && dz > -280 && dz < -5  
315 && abs(dpx) < 1.8 && abs(dpy) < 2 && dpx*dpx + dpy*dpy < 5 && dpz > 38  
316 && dpz < 116 && dx*dx + (dy-beamOffset)*(dy-beamOffset) < 0.06  
317 && abs(trackSeparation) < 270 && chisq_dimuon < 18  
318 && abs(chisq1_target + chisq2_target - chisq_dimuon) < 2  
319 && y1_st3*y2_st3 < 0 && nHits1 + nHits2 > 29 && nHits1St1 + nHits2St1 > 8  
320 && abs(x1_st1+x2_st1) < 42
```

321 **A.4 Physics and Occupancy Cuts**

```
322 // physicsCuts_2111v42  
323 mass > 4.2 && xF > 0 && xF < 0.8 && pt < 5 && pt > 0.1  
324 && abs(pz1_st1-pz2_st1) < 50 && abs(px1_st1-px2_st1) < 3.5  
325 && abs(py1_st1-py2_st1) < 3.5 && pz1_st1 > 15 && pz2_st1 > 15  
326 && pz1_st1 < 75 && pz2_st1 < 75  
327  
328 // occCuts_2111v42  
329 D1 < 150 && D2 < 150 && D3 < 150 && D4 < 150
```

³³⁰ **Acknowledgements**

³³¹ The authors wish to express their gratitude to **Kenichi Nakano (University of Virginia)** and
³³² **Ching Him Leung (Jefferson Laboratory)** for insightful discussions and valuable feedback.
³³³ We also thank **Shivangi Prasad (University of Illinois Urbana-Champaign)** and **Harsha**
³³⁴ **Kaluarachchi (New Mexico State University)** for their helpful conversations and support
³³⁵ throughout this work.

³³⁶ **References**

- ³³⁷ [1] S. D. Drell and T.-M. Yan, *Massive Lepton-Pair Production in Hadron-Hadron Collisions at High Energies*, Phys. Rev. Lett. **25**, 316 (1970).
- ³³⁸
- ³³⁹ [2] An alternative proposal for determining DY yields. DocDB 11322-v1